frontiers | Frontiers in Marine Science

TYPE Original Research
PUBLISHED 12 June 2023
DOI 10.3389/fmars.2023.1196906

OPEN ACCESS

EDITED BY
Yifei Zhao,
Nanjing Normal University, China

REVIEWED BY
Fajin Chen,
Guangdong Ocean University, China
Zhiyong Liu,
Soochow University, China

*CORRESPONDENCE
Dongliang Lu
ldl@bbgu.edu.cn

RECEIVED 31 March 2023
ACCEPTED 17 May 2023
PUBLISHED 12 June 2023

CITATION
Wang X, Zhou J, Su K, Du J, Wei L, Li X, Du J and Lu D (2023) Atmospheric radioactive nuclide deposition on the coast of the Maowei Sea, northern Beibu Gulf, China. *Front. Mar. Sci.* 10:1196906. doi: 10.3389/fmars.2023.1196906

Atmospheric radioactive nuclide deposition on the coast of the Maowei Sea, northern Beibu Gulf, China

Xilong Wang[1,2], Jiaodi Zhou[1], Kaijun Su[3], Jinzhou Du[4], Longtao Wei[1], Xing Li[1], Juan Du[5] and Dongliang Lu[1]*

[1]Guangxi Key Laboratory of Marine Environmental Change and Disaster in Beibu Gulf, Beibu Gulf University, Qinzhou, China, [2]School of Geographic and Environmental Sciences, Tianjin Normal University, Tianjin, China, [3]Institute of Radiation Medicine, Chinese Academy of Medical Sciences and Peking Union Medical College, Tianjin, China, [4]State Key Laboratory of Estuarine and Coastal Research, East China Normal University, Shanghai, China, [5]Research Centre for Eco-Environmental Engineering, Dongguan University of Technology, Dongguan, China

The natural radioisotopes ^{7}Be, ^{210}Pb, and ^{210}Po, with different half-lives, are all particle-reactive and serve as natural tracers to study sources and transportation of sediments, sedimentation rates, and sediment chronology. Atmospheric deposition of these radioisotopes is the premise and foundation of their tracing application. The Maowei Sea is a semi-closed bay along the Beibu Gulf, which is an important gulf in the northwest of the South China Sea, but the atmospheric deposition of the abovementioned radioisotopes has not been systematically reported along the coast. In this research paper, the atmospheric depositional fluxes of ^{7}Be, ^{210}Pb, and ^{210}Po were observed over a period from June 2018 to December 2021 on the coast of the Maowei Sea. The annual atmospheric depositional fluxes (Bq m^{-2} yr^{-1}) of ^{7}Be, ^{210}Pb, and ^{210}Po on the coast of the Maowei Sea were 496.80, 201.72, and 58.08, respectively. The distributions for ^{7}Be and ^{210}Pb depositional fluxes during a whole year (years 2019 and 2021) followed a bimodal pattern, with one peak from February to April and another peak from August to October, while the distribution for ^{210}Po depositional flux showed only one peak during the year of 2019 and another during 2021. The deposition flux and activity of ^{7}Be showed a strong positive correlation with the deposition flux and activity of ^{210}Pb, respectively; the deposition flux and activity of ^{210}Po also showed positive correlations with the deposition fluxes and activities of ^{210}Pb and ^{7}Be, respectively, indicating a similarly scavenging behavior from the atmosphere. A Pearson correlation matrix was used to illustrate the factors influencing the atmospheric depositions and found that precipitation, air quality index (AQI), and PM (both $PM_{2.5}$ and PM_{10}) were the major factors that influenced the deposition of these three radionuclides. Precipitation had significant positive correlations with the deposition fluxes of all three radionuclides, indicating that, for these radionuclides, rainfall was the main scavenging way from the atmosphere. The

10.3389/fmars.2023.1196906

observations for specific single rainfall events and their air mass backward trajectory analyses showed that the air masses movement during the rainfall may be another important factor that impacted the depositional fluxes for ^{7}Be, ^{210}Pb, and ^{210}Po.

KEYWORDS

atmospheric deposition, ^{7} Be, ^{210} Pb, ^{210} Po, activity ratio, Maowei Sea

1 Introduction

Radionuclides widely exist in the environment and are involved in various biogeochemical processes. Because of different sources and half-lives, nuclides of the natural decay chains are widely applied to atmospheric research, oceanography, and marine geology (Du et al., 2008). ^{7}Be, ^{210}Pb, and ^{210}Po are natural radionuclides that have been widely used as tracers and chronometers in aquatic, sedimentary, and atmospheric systems (e.g. McNeary and Baskaran, 2007; Du et al., 2010; Chen et al., 2016; Su et al., 2017; Du et al., 2020). ^{7}Be ($T_{1/2}$ = 53.3 days), ^{210}Pb ($T_{1/2}$ = 22.3 years), and ^{210}Po ($T_{1/2}$ = 138 days) have different half-lives, but they are all particle-reactive. Thus, they can be used as natural tracers to study the source and transportation of sediments, sedimentation rates, sediment chronology, atmospheric depositional fluxes, and residence time of atmospheric aerosols (e.g. Turekian et al., 1977; Zou et al., 1982; McKee et al., 1983; DeMaster et al., 1985; Qian et al., 1986; Feng et al., 1999a; Feng et al., 1999b; Fornes et al., 1999; Baskaran and Swarzenski, 2007; McNeary and Baskaran, 2007; Du et al., 2010; Huang et al., 2010; Shan, 2010; Baskaran, 2011; Dai et al., 2011; Huang et al., 2013; Du et al., 2016; Du et al., 2020).

^{7}Be is a typical radionuclide produced by cosmic rays bombarding nitrogen and oxygen atoms in the atmosphere (Lal et al., 1958). The main factors affecting its generation are the activity cycles of sunspots, altitude, and latitude. (Lal and Peters, 1967). Approximately 70% of ^{7}Be in the atmosphere is generated at the bottom of the stratosphere and 30% at the top of the troposphere. Once generated, ^{7}Be will be tightly adsorbed to the atmospheric particles, and the residence time of particles in the stratosphere is approximately 1 year, which is much longer than the half-life of ^{7}Be (Dutkiewicz and Husain, 1985). Therefore, most of the ^{7}Be produced in the stratosphere does not reach the troposphere except during spring (mostly in the mid-latitudes), resulting in ^{7}Be that sinks to the Earth's surface coming mainly from the troposphere. After its generation in the atmosphere, ^{7}Be will be quickly adsorbed to the submicron particles and arrive at the earth's surface by wet and dry deposition and participate in a series of geochemical processes (Wallbrink and Murray, 1994; Zhu and Olsen, 2009). At the same time, ^{7}Be suffers from its self-radioactive decay. Due to the particle's active and clear source, ^{7}Be is widely used to trace atmospheric processes and geochemical processes, such as particulate transport over a time scale of approximately 200 days (Zheng et al., 2010; Shi et al., 2011; Huang, 2012).

While ^{210}Pb is produced by radioactive decay from its progenitor, ^{222}Rn, which is a noble gas isotope in the ^{238}U decay chain, emanates primarily from rocks and minerals on the land surface including continent and ocean, and escapes into the atmosphere (Moore et al., 1973; Baskaran et al., 1993; Du et al., 2020). ^{210}Po is generated from ^{210}Pb *via* ^{210}Bi ($T_{1/2}$ = 5.0 d). Similar to ^{7}Be, both ^{210}Pb and ^{210}Po are easily adsorbed by atmospheric particles of sub-micron scale, and then reach the Earth's surface *via* dry and wet deposition and are finally buried in sediments (Peirson et al., 1966; Baskaran, 2011). In the absence of ^{210}Po from sources other than the radioactive decay of atmospheric ^{222}Rn-derived ^{210}Pb, the ^{210}Po/^{210}Pb activity ratio (AR) usually can be utilized to determine the age of aerosols, particles, snow, melt pond, ice core, etc. (Moore et al., 1973; Robbins, 1978; Nozaki et al., 1997; Marley et al., 2000; Baskaran and Santschi, 2002; Huang, 2012; Du et al., 2016; Baskaran and Krupp, 2021).

Although ^{7}Be, ^{210}Pb, and ^{210}Po have different sources, they are all atmospheric fallout radioactive isotopes. The prerequisite for their tracer application is a deep understanding of their atmospheric deposition characteristics and deposition fluxes. In China, there have been some reports on the atmospheric deposition of ^{7}Be, ^{210}Pb, and ^{210}Po (Table 1), but these studies mainly focused on the eastern coastal areas of China, and there was less data on the study of the three isotopes simultaneously. As an important bay in the northwest of the South China Sea, the atmospheric deposition flux of radioisotopes along the coast of the Beibu Gulf is also worth attention. This is of great significance for a deeper understanding of the source-sink pattern of radioactive isotopes in the South China Sea. However, studies on the atmospheric deposition of ^{7}Be, ^{210}Pb, and ^{210}Po along the Beibu Gulf are very limited and have not been reported previously. The Maowei Sea is a typical subtropical bay facing the Beibu Gulf (Figure 1) and is located in the southern part of Qinzhou, Guangxi, China (Figure 1), which is one of the land-sea node cities in the southward channel of "the Belt and Road" initiative. Thus, according to "the Belt and Road" national strategy and regional advantages, it is necessary to pay more attention to the atmospheric environment on the coast of the Maowei Sea. Besides, this study site is suitable for investigating the boundary layer outflow of continental pollution to the Beibu Gulf region. Therefore, in this study, the depositional characteristics of ^{7}Be, ^{210}Pb, and ^{210}Po were studied during a long period on the

TABLE 1 A summary of atmospheric depositional fluxes of ^{7}Be, ^{210}Pb, and ^{210}Po in China.

Study area	Sampling date	Longitude	Latitude	Annual precipitation	^{7}Be atmospheric depositional flux	^{210}Pb atmospheric depositional flux	^{210}Po atmospheric depositional flux	Reference
		°E	°N	mm	Bq m^{-2} d^{-1}	Bq m^{-2} d^{-1}	Bq m^{-2} d^{-1}	
Changchun	2012.08-2013.07	125.19	43.54	570	0.59-4.33 (1.91)	–	–	Gai et al., 2015
Beijing	2012.08-2013.07	116.4	39.54	644	0.09-8.25 (3.90)	–	–	
Ansai	2010.4-2012.12	109.3	36.86	483	3.57-6.08 (4.82)	–		Zhang et al., 2013
Qingdao	2002.4-2002.11	120.33	36.06	421	1.02-2.97 (1.67)	0.25-0.43 (0.32)	–	Yi et al., 2005
	2004.5-2004.9	120.33	36.06	376	1.54-2.60 (2.15)	0.33-0.68 (0.51)	0.027-0.187 (0.083)	
	2012.08-2013.07	120.47	35.85	720	0.29-7.48 (2.45)	–	–	Gai et al., 2015
Nanjing	2010.1-2011.12	118.91	32.12	1101	0.66-14.5 (4.44)	–	–	Yang et al., 2012
Shanghai	2006-2016	121.4	31.23	1168	3.19-5.59 (4.39)	0.87-1.71 (1.16)	–	Du et al., 2008; Du et al., 2015; Du, 2019
	2016.7-2018.4	121.4	31.23	858	(2.84 ± 0.37)	(0.69 ± 0.11)	(0.06 ± 0.02)	Zhong, 2020
Three Gorges Reservoir	2009.5-2010.5	108.2	30.4	1026	0.4-5.2 (2.6)	–	–	Shi et al., 2011
Hangzhou	2012.08-2013.07	120.13	30.29	1454	1.02-4.67 (1.94)	–	–	Gai et al., 2015
Yueyang	2012.1-2012.12	113.02	29.35	1584	0.81-2.95 (2.30)	0.16-0.63 (0.45)	–	Peng et al., 2019
	2016.1-2016.12	113.02	29.35	1284	0.51-3.26 (1.84)	0.14-0.65 (0.41)	–	
Hengyang	2012.1-2012.12	112.58	26.77	1356	0.94-3.89 (2.13)	0.32-1.26 (0.76)	–	
	2016.1-2016.12	112.58	26.77	1284	0.64-3.98 (2.00)	0.41-1.31 (0.93)	–	
Peng-Chia Yü	1996-2001	122.1	25.7	1929	0.00-11.46 (3.06)	0.00-1.81 (0.50)	–	Su et al., 2003
Nankang	1996-2001	121.6	25	1945	0.60-13.3 (5.02)	0.00-1.83 (0.87)	–	
Taiwan	1996.10-2014.1	121.61	25.04	2784	0.06-48.56 (5.77)	0.02-9.56 (1.25)	–	Lee et al., 2015
Xiamen	2001.8-2002.8	118.1	24.4	1618	0.21-3.52 (1.90)	0.10-1.11 (0.41)	–	Jia et al., 2003
	2004.3-2005.4	118.08	24.43	1135	0.11-2.93 (1.64)	0.04-0.85 (0.51)	0.002-0.133 (0.061)	Yi et al., 2007
	2010.11-2012.1	118.1	24.44	800.4	–	0.08-0.98 (0.51)	0.005-0.113 (0.039)	Wang et al., 2014
	2013.1-2014.12	118	24.5	1250	–	0.00-4.15 (0.78)	0.002-0.403 (0.065)	Zhang et al., 2019

(Continued)

TABLE 1 Continued

Study area	Sampling date	Longitude	Latitude	Annual precipitation	^{7}Be atmospheric depositional flux	^{210}Pb atmospheric depositional flux	^{210}Po atmospheric depositional flux	Reference
		°E	°N	mm	Bq m^{-2} d^{-1}	Bq m^{-2} d^{-1}	Bq m^{-2} d^{-1}	
Dongshan Bay Coast	2021.01-2022.01	117.54	23.93	687	–	0.07-0.99 (0.46)	0.026-0.394 (0.104)	Zhong et al., 2023
Guangzhou	2012.08-2013.07	113.31	23.10	1736	0.14-6.12 (1.32)	–	–	Gai et al., 2015
Shenzhen	2015.1-2015.12	113.94	22.54	1400.8	0.91~4.23 (1.83)	–	–	Ding et al., 2017
	2017.1-2017.12	113.94	22.54	1856.1	–	0.45-1.31 (0.74)	–	Wu et al., 2021
	2015.1-2018.1	113.94	22.54	1933	0.25-3.54 (1.55)	0.45-1.31 (0.77)	–	Su, 2018
Maowei Sea Coast	2018.6-2021.12	108.61	21.9	2765	0.14-3.45 (1.38)	0.06-1.43 (0.56)	~0-1.15 (0.16)	This study

-, Not available.

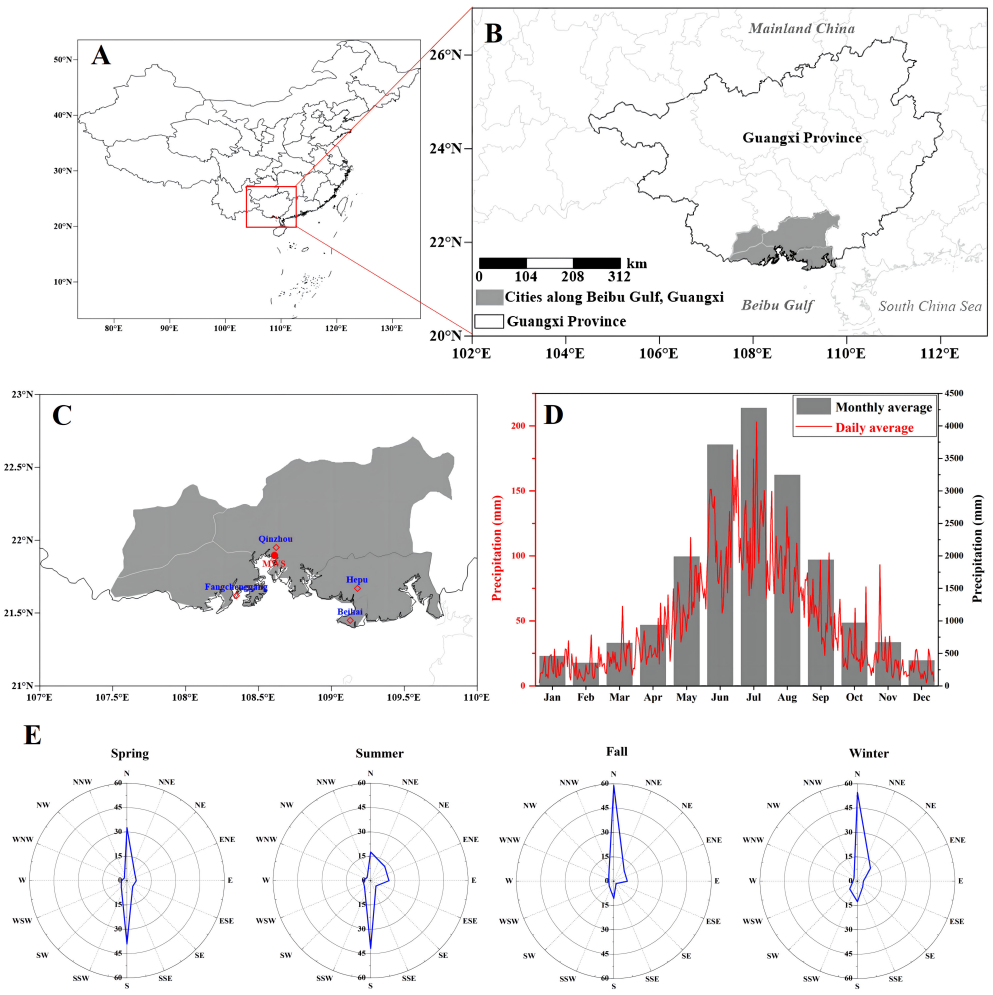

FIGURE 1
Location of Guangxi Province **(A, B)**, study site, and monitoring stations of air quality and meteorological factors along Beibu Gulf, Guangxi **(C)**. 20-year (2000-2019) average of daily and monthly precipitation at the Qinzhou site **(D)** from National Data Center for Meteorological Sciences. The wind-rose diagram from June 2018 to December 2021 for the Qinzhou site (**E**, data from https://www.weatheronline.co.uk/).

coast of the Maowei Sea to reveal the atmosphere-sea surface interactions in the Beibu Gulf. The present study is also the first observation of the radioactive nuclides' depositional fluxes along the Beibu Gulf in southern China.

2 Study site

The Maowei Sea belongs to the inner Qinzhou Bay, with an average water depth of ~2.5 m. The surface area of the Maowei Sea is ~135 km^2 with two major rivers (Maoling River and Qin River) discharging into the bay from the north. The tides of the Maowei Sea are irregular and diurnal, with a wide range of 0.05-4.04 m (Chang et al., 2015). The Maowei Sea is located in the south of Qinzhou City and is an important aquaculture bay for the life of people in Qinzhou. Qinzhou is an important city in the Beibu Gulf urban agglomeration. It is located on the southwest coast of Guangxi at 21°35′-22°41′ N and 107°72′-109°56′ E adjacent to the Maowei Sea (Figure 1). Qinzhou is bordered by the Beibu Gulf in the south and thousands of mountains in the northwest, hence it is affected both by marine and land air masses. In the monsoon region of southeast Asia, Qinzhou is strongly influenced by solar radiation and the monsoon circulation. The climate is classified as tropical maritime monsoon, and the rainy season is between May and September. A figure for the 20-year (from 2000 to 2019) average of daily and monthly precipitation at the Qinzhou site (Figure 1C) from the National Data Center for Meteorological Sciences is shown in Figure 1D. The wind-rose diagram during our sampling period for the Qinzhou site (Figure 1E, data from https://www.weatheronline.co.uk/) showed that the dominant wind direction during the sampling period was south during the summer, north during the fall and winter, and south and north during the spring.

3 Sampling and methods

Samples were collected from June 2018 to December 2021 from the roof of the Ocean Building at Beibu Gulf University, which was built on the coast of the Maowei Sea, at ~20 m above ground level (Figure 1C, site named MWS, 21.8975°N, 108.6083°E, ~25 m above mean sea level). At this height, the contribution of ^{7}Be, ^{210}Pb, and ^{210}Po from resuspended dust from the local ground area is assumed negligible (Du et al., 2015). Wet and dry depositional samples were collected at monthly intervals by a rainwater collector (a steel container with a ceramic painting surface) with a surface area of 1.44 m^2. At the same time, single rainfall events in the rainy season during the year 2019 were also collected to identify the contributions of the single rainfall events and analyze the influence of the climate factors.

After the samples were collected, the dilute HNO_3 was used to rinse the surface of the container to prevent the loss of ^{7}Be, ^{210}Pb, and ^{210}Po by adsorption onto the container walls. The daily precipitation data were obtained from the National Meteorological Information Center (https://data.cma.cn/). Co-precipitation of ^{7}Be, ^{210}Pb, and ^{210}Po from rainwater was obtained by $Fe(OH)_3$ (Du et al., 2008; Du et al., 2015). Briefly, after collection, the rainwater samples were acidified to pH~2 with concentrated HNO_3. Then 1 mg stable Pb^{2+} (in the form of $Pb(NO_3)_2$) and 1 mg Be^{2+} (in the form of $BeSO_4$) were added for the determination of chemical yield. A known amount of iron ion (5 mg Fe^{3+} per liter sample) in the form of $FeCl_3$ was added to the solution. Then, 10 hours later, the pH of the solution was adjusted to ~8 by adding ammonium hydroxide. The $Fe(OH)_3$ precipitation was allowed to settle, and the supernatant and precipitate were separated by centrifugation. The residue was freeze-dried before measurement. As has been reported before (Du et al., 2008), the co-precipitate efficiency of this method was approximately 96% and 99% for ^{7}Be and ^{210}Pb, respectively.

The activities of ^{7}Be and ^{210}Pb in the samples were measured by an HPGe gamma-ray detector system (50% relative efficiency, Canberra GX5019) after the dried residue was quantitatively transferred into a plastic box (70×35 mm). The activities of ^{210}Pb (46.5 KeV, 4.25%) and ^{7}Be (477.6 KeV, 10.5%) were obtained from the counting of the samples for 24 h. The efficiency calibration curve was obtained by LabSOCS with efficiency uncertainties of less than 7% for ^{7}Be and 10% for ^{210}Pb (Bronson, 2003; Wu et al., 2009). During the deployment period, ^{7}Be was continuously added by wet and dry precipitation from the first day of collection, but at the same time, it also underwent radioactive decay. Thus, the ^{7}Be depositions were corrected for radioactive decay from the middle time of the collection date to the mid-counting time (Kim et al., 1998). Since there was a relatively long half-life, the correction of radioactive decay for ^{210}Pb was negligible.

After collection, samples for ^{210}Po were analyzed in the laboratory following the description made by Zhong et al. (2019); Zhong et al. (2020). Briefly, the water samples were immediately filtered through 0.45 μm membrane filters and stirred vigorously for 30 minutes to remove the residual ^{222}Rn gas. The filtered samples were acidified immediately to pH 1~2 with HNO_3 and soon after spiked with ~1 dpm of ^{209}Po. Then, Po was coprecipitated with Fe $(OH)_3$. After settling and centrifugation, the supernatant was discarded and the precipitate was dissolved. After adjusting pH to 1.5~2 and adding 1 ml 20% hydroxylamine hydrochloride, 1 ml 25% Citrate sodium, and 0.3 g Ascorbic acid, Po isotopes were auto-deposited onto nickel disks immersed in the solution. The ^{209}Po and ^{210}Po were measured using a low background α-spectrometer (Alpha Analyst, AlphEnsembol-8, TE). The treatment method of particulate ^{210}Po on the filter membrane was digested on the heating plate after adding HCl for acidification and ~1 dpm ^{209}Po (weigh the spike to get the extract amount) as a tracer. Because of the black carbon in the sample, the sample could never be digested clearly, so used a filter membrane to filter and collect the solution. Then, the solution was treated the same as the dissolved precipitate for the dissolved ^{210}Po.

The estimation of depositional fluxes for ^{7}Be, ^{210}Pb, and ^{210}Po in this study was based on the variations of nuclides' activities with time (Jia et al., 2003; Bi, 2013). During the sampling period for a specific sample, the radioactive nuclides were added through wet and dry precipitation continuously, but the radioactive self-decay happened at the same time. Thus, the activity of a specific radioactive nuclide over time can be expressed as:

$$\frac{da}{dt} = sf - \lambda a \quad (1)$$

Where, A is the activity of a specific nuclide; t is the elapsed time; S is the surface area of the rainwater collector; F is the depositional flux of a specific nuclide; λ is the decay constant of the specific nuclide. Assuming the depositional flux was stable during the sampling period for the monthly sample/single rainfall sample, the activity of nuclide in the collector after a collecting time of t_1 can be expressed by:

$$A_{t_1} = \frac{SF}{\lambda} \times (1 - e^{-\lambda t_1}) \quad (2)$$

If the sample was measured at t_2, then the measured activity can be given as:

$$A_{t_2} = A_{t_1} \times e^{-\lambda t_2} = \frac{SF}{\lambda} \times (1 - e^{-\lambda t_1}) e^{-\lambda t_2} \quad (3)$$

Then, the depositional flux can be given as:

$$F = \frac{A_{t_2} \times \lambda \times e^{\lambda t_2}}{S \times (1 - e^{-\lambda t_1})} \quad (4)$$

Equation (4) can be used to estimate the monthly depositional flux for ^{7}Be. However, for ^{210}Pb, the correction for its radioactive self-decay can be negligible because of its long half-life. Therefore, equation (4) for ^{210}Pb can be simplified as the following equation.

$$F = \frac{A_{t_2}}{S \times t_1} \quad (5)$$

For ^{210}Po, in addition to its self-decay, it was necessary to correct the contribution from its parent. Because of the short half-life of ^{210}Bi ($T_{1/2}$ = 5 days), it could be considered that ^{210}Pb and ^{210}Bi were in equilibrium during the sampling period. Thus,

$$\frac{dA_{Po}}{dt} = SF_{Po} - \lambda_{Po} A_{Po} + \lambda_{Po} A_{Pb} \quad (6)$$

Then, the depositional flux for ^{210}Po can be given as:

$$F_{Po} = \frac{\lambda_{Po}}{S \times (1 - e^{-\lambda_{Po} t_1})} \left[A_{Po} - \frac{SF_{Pb}}{\lambda_{Pb}} (1 - e^{-\lambda_{Po} t_1}) - \frac{\lambda_{Po} SF_{Pb}}{(\lambda_{Po} - \lambda_{Pb}) \lambda_{Pb}} (e^{-\lambda_{Po} t_1} - e^{-\lambda_{Pb} t_1}) \right] \quad (7)$$

The volume-weighted activity of a specific nuclide (A_V) in the atmosphere can be estimated based on the total amount of the nuclide divided by the rainfall data. Thus, the volume-weighted activity can be expressed as:

$$A_V = \frac{F \times t_1}{P} \quad (8)$$

where, P is the precipitation during the sampling period (mm).

4 Results and discussion

4.1 Precipitation and air quality

During the study period, the mean annual total precipitation was 2765 mm, and the average air quality index (AQI) showed an excellent air quality rating. The average concentrations (μg/m^3) for $PM_{2.5}$ and PM_{10} in the air during the sampling period were 26.49 and 46.78, respectively. No significant differences (p>0.05) were found among different sampling years for all these factors (precipitation, AQI, $PM_{2.5}$, PM_{10}). As seen in Figure 2, the monthly precipitation varied contrary to the levels of $PM_{2.5}$ (r=-0.624, p<0.01), PM_{10} (r=-0.622, p<0.01), and AQI (r=-0.633, p<0.01), and AQI varied consistent with the levels of $PM_{2.5}$ (r=-0.991, p<0.01) and PM_{10} (r=-0.987, p<0.01). This indicated that the precipitation might be the major factor influencing the scavenging of PM in the study area and affected the air quality further.

4.2 Atmospheric deposition of ^{7}Be, ^{210}Pb, and ^{210}Po

The calculation of monthly deposition fluxes for ^{7}Be, ^{210}Pb, and ^{210}Po were based on equations (4), (5), and (7), respectively. During our sampling period, the monthly deposition fluxes (Bq m^{-2} month^{-1}) of ^{7}Be varied from 4.16 to 103.58 with a mean of 41.40 (n=38). No significant difference (p>0.05) was observed among different sampling years. The annual ^{7}Be deposition flux was estimated to be 496.80 Bq m^{-2} yr^{-1}, which was within the low level of the global reported data range (409-5300 Bq m^{-2} yr^{-1} from 19.0°N to 47.7°N, Du et al., 2015).

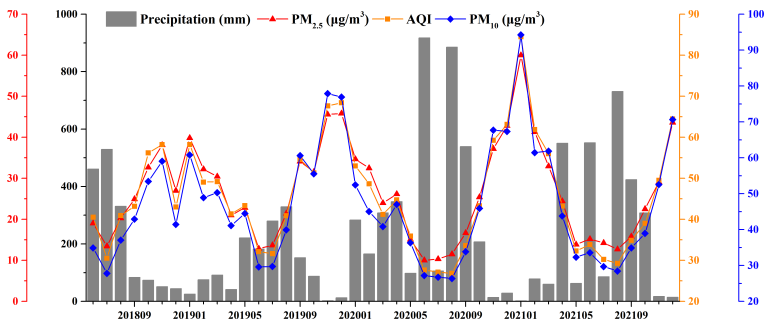

FIGURE 2
Monthly variation of precipitation, AQI, and concentrations of $PM_{2.5}$ and PM_{10} during the sampling period.

In China, this observation result was close to the reported data in Guangzhou but lower than other sites with a higher latitude than this study region (Table 1). The atmospheric deposition ^{7}Be flux was expected to have a latitudinal variation since it originated from the interaction between cosmic rays and the atmosphere. Some studies found this to be the case (Turekian et al., 1983; McNeary and Baskaran, 2003; Usoskin and Kovaltsov, 2008; Du et al., 2015; Zhong, 2020). Our study site was at a low latitude of 21.9°N but higher than the deposition flux in Spain (36-37°N), indicating that in addition to its different production rate with latitude, other factors, such as air convection, precipitation, and residence time of airborne particles, might affect the atmospheric deposition ^{7}Be flux. From June 2018 to December 2021, the atmospheric depositional ^{210}Pb fluxes (Bq m^{-2} month^{-1}) varied from 1.92 to 42.82 with an average of 16.81 (n=38) on the Maowei Sea coast. A significant difference (p<0.05) was found between different sampling years (June 2018-July 2019 and June 2020-July 2021). The mean deposition flux was higher during June 2018-July 2019 than in June 2020-July 2021. As is widely known, the COVID outbreak reached epidemic proportions at the end of 2019. The ^{210}Pb in the atmosphere mainly comes from the emanation of ^{222}Rn, 99% of which in the atmosphere originates from the continent (Baskaran, 2011). Thus, the lower deposition flux in the later year may be due to reduced human and terrestrial activities caused by the COVID-19 pandemic and which had not yet been fully restored. As reported, the GDP decreased by 6.8% from the last quarter of 2019 to the first quarter of 2020, and the unemployment rate of residents increased to 6.2% in February 2020 (Xia et al., 2020). Whereas, the urban pollutants were reduced especially for the concentrations of $PM_{2.5}$ and PM_{10} with a decrease of 48% and 47%, respectively (Wu et al., 2020). The mean annual ^{210}Pb deposition flux was estimated to be 201.72 Bq m^{-2} yr^{-1}, which was among the global ^{210}Pb deposition flux range (59-840 Bq m^{-2} yr^{-1}, Du et al., 2015; Zhong, 2020). In China, the ^{210}Pb deposition flux on the Maowei Sea Coast was close to the average reported value (255 Bq m^{-2} yr^{-1}, Table 1). A significant linear relationship was found between the deposition fluxes of ^{210}Pb and ^{7}Be (r=0.887, p<0.01, n=38), indicating a similar atmospheric environment behavior path for ^{210}Pb and ^{7}Be (Jia et al., 2003; McNeary and Baskaran, 2003). During the study period, the atmospheric deposition fluxes (Bq m^{-2} month^{-1}) of ^{210}Po ranged from ~0 to 34.35 with an average of 4.84 (n=38). Similarly, a significant difference (p<0.05) was found for ^{210}Po deposition flux between different sampling years (June 2018-July 2019 and June 2020-July 2021). A much lower ^{210}Po deposition flux was obtained during June 2020-July 2021 than during June 2018-July 2019. Since the ^{210}Po in the atmosphere mainly comes from the decay of ^{210}Pb, the COVID-19 pandemic might also have influenced the production of ^{210}Po, consequently influencing its deposition flux. The mean annual ^{210}Po deposition flux was estimated to be 58.08 Bq m^{-2} yr^{-1}, which was among the global ^{210}Po deposition flux range (11.40-83.46 Bq m^{-2} yr^{-1}, Zhong, 2020), but higher than ever reported data in China (11.40-20.60 Bq m^{-2} yr^{-1}, Table 2). In general, the atmospheric deposition of ^{210}Po showed a defect compared to ^{210}Pb, which may be due to the short residence time of ^{210}Pb in the atmosphere, which makes it difficult to produce enough ^{210}Po. Linear relationships were found between the deposition fluxes of ^{210}Po and ^{7}Be (r=0.449, p<0.01, n=38) and between ^{210}Po and ^{210}Pb (r=0.310, p=0.058, n=38), but they were not significant, indicating a different atmospheric environment behavior of ^{210}Po.

The temporal variations of monthly deposition fluxes for ^{7}Be, ^{210}Pb, and ^{210}Po during the study period are shown in Figure 3A. Due to the special circumstance caused by COVID-19, no data was available from January to May 2020. From Figure 3A, we can see that the highest ^{7}Be deposition flux value was observed in April 2021 and the lowest value was in November 2019; it was also much lower in November 2020. The highest ^{210}Pb deposition flux value was observed in August 2018 and the lowest value was in November 2020. The highest monthly deposition flux of ^{210}Po was shown in February 2019. Except for February, March, and April 2019, the deposition flux of ^{210}Po was much lower than 10 Bq m^{-2} month^{-1} and even near zero in several months, which indicated that ^{210}Po mainly came from the decay of ^{210}Pb and the residence time of ^{210}Pb in the atmosphere was short, making it difficult to produce enough ^{210}Po. The high deposition flux in February, March, and April may be due to the special high-humidity weather that is experienced in Guangxi, China from February to April. The special high-humidity weather is called “Huinan Tian” in Chinese and usually occurs after a long-term cold air in spring. During this, temperature and humidity increase suddenly, atmospheric pressure decreases suddenly, and the air becomes saturated (Luo et al., 2015; Huang et al., 2020). Under the influence of “Huinan Tian”, water vapor in the air condenses into small water drops, which can carry more ^{7}Be, ^{210}Pb, and ^{210}Po during each rainfall event because of a relatively larger surface area per unit mass. Such cases are very similar to the plum rain season in Shanghai, China (Yang et al., 2005; Du, et al., 2015).

This special weather made the atmospheric deposition much slower in order to produce more ^{210}Po in the air. The deposition fluxes of ^{7}Be, ^{210}Pb, and ^{210}Po varied a lot in the same month of different years, with a maximum coefficient of variation of 100%, 101%, and 149% for ^{7}Be, ^{210}Pb, and ^{210}Po, respectively, and a minimum coefficient of variation of 13%, 8%, and 36% for ^{7}Be, ^{210}Pb, and ^{210}Po, respectively. The monthly deposition flux varied most in November for both ^{7}Be and ^{210}Pb, and in December for ^{210}Po; and varied least in April for both ^{7}Be and ^{210}Pb, and in August for ^{210}Po. The overall variation trends for ^{7}Be, ^{210}Pb, and ^{210}Po deposition fluxes showed high values from June to October and from February to April, and low values from November to February. If we analyze the data from January 2019 to December 2019, and from January 2021 to December 2021, it becomes clear that the distribution of ^{7}Be and ^{210}Pb deposition fluxes followed a bimodal pattern, with one peak from February to April and another peak from August to October. While the distribution of ^{210}Po deposition flux was similar to an irregular parabola, with the peak showing from August to October 2019 and from February to April 2021.

The distribution of seasonal deposition fluxes for ^{7}Be, ^{210}Pb, and ^{210}Po are shown in Figure 3B. The seasonal deposition fluxes ranged from 52.18 to 245.93 (mean=128.97, n=12) Bq m^{-2} season^{-1} for ^{7}Be, from 23.48 to 109.48 (mean=52.36, n=12) Bq m^{-2} season^{-1} for ^{210}Pb, and from 0.36 to 47.78 (mean=15.18, n=12) Bq m^{-2}

10.3389/fmars.2023.1196906

TABLE 2 Depositional fluxes and activities of ^{7}Be, ^{210}Pb, and ^{210}Po measured in the single rainfall events on the coast of the Maowei Sea during 2019.

Sample ID	Sampling date	Collection time interval (d)	Depositional flux (Bq m^{-2} d^{-1})			Volume-weighted activity (Bq L^{-1})			Precipitation (mm)	$^{7}Be/^{210}Pb$ AR	$^{210}Po/^{210}Pb$ AR
			^{210}Pb	^{7}Be	^{210}Po	^{210}Pb	^{7}Be	^{210}Po			
R-1	20190615	1.0	0.361	0.706	0.062	0.027 ± 0.004	0.052 ± 0.003	0.0045 ± 0.0006	14.2	1.96	0.171
R-2	20190616	0.9	5.340	23.970	0.360	0.116 ± 0.017	0.522 ± 0.031	0.0079 ± 0.0012	42.0	4.49	0.067
R-3	20190617	0.9	0.621	2.745	0.058	0.032 ± 0.005	0.143 ± 0.009	0.0030 ± 0.0004	17.3	4.42	0.094
R-4	20190618	1.0	0.373	1.593	0.033	0.153 ± 0.023	0.653 ± 0.039	0.0135 ± 0.0014	2.5	4.27	0.088
R-5	20190620	2.0	1.047	1.939	0.130	0.060 ± 0.009	0.112 ± 0.007	0.0075 ± 0.0011	34.1	1.85	0.124
R-6	20190701	1.7	1.121	4.113	0.083	0.031 ± 0.005	0.112 ± 0.007	0.0024 ± 0.0003	61.9	3.67	0.074
R-7	20190703	2.0	0.115	0.308	0.034	0.012 ± 0.002	0.032 ± 0.002	0.0035 ± 0.0005	19.3	2.67	0.293
R-8	20190704	0.4	0.780	1.526	0.147	0.056 ± 0.008	0.110 ± 0.007	0.0106 ± 0.0011	5.4	1.96	0.189
R-9	20190709	4.9	0.151	0.431	0.016	0.064 ± 0.010	0.183 ± 0.011	0.0066 ± 0.0013	11.6	2.85	0.103
R-10	20190710	0.9	0.476	0.567	0.098	0.044 ± 0.007	0.052 ± 0.003	0.0091 ± 0.0009	10.2	1.19	0.207
R-11	20190713	2.9	0.385	1.131	0.035	0.063 ± 0.009	0.186 ± 0.011	0.0057 ± 0.0005	17.5	2.94	0.090
R-12	20190714	1.1	3.587	17.114	0.287	0.125 ± 0.019	0.595 ± 0.036	0.0100 ± 0.0011	32.4	4.77	0.080
R-13	20190804	1.2	1.026	1.280	0.924	0.054 ± 0.008	0.067 ± 0.004	0.0482 ± 0.0029	22.6	1.25	0.900
R-14	20190817	12.7	0.248	0.934	0.047	0.082 ± 0.012	0.309 ± 0.019	0.0156 ± 0.0018	38.3	3.77	0.191
R-15	20190820	3.0	0.442	3.253	0.077	0.214 ± 0.032	1.573 ± 0.094	0.0374 ± 0.0032	6.2	7.35	0.175
R-16	20190823	3.0	0.686	2.767	0.088	0.347 ± 0.052	1.401 ± 0.084	0.0445 ± 0.0044	5.9	4.03	0.128
R-17	20190826	3.2	2.264	5.688	0.343	1.936 ± 0.290	4.863 ± 0.292	0.2935 ± 0.0136	3.7	2.51	0.152

(Continued)

TABLE 2 Continued

Sample ID	Sampling date	Collection time interval (d)	Depositional flux (Bq m^{-2} d^{-1})			Volume-weighted activity (Bq L^{-1})			Precipitation (mm)	$^{7}Be/^{210}Pb$ AR	$^{210}Po/^{210}Pb$ AR
			^{210}Pb	^{7}Be	^{210}Po	^{210}Pb	^{7}Be	^{210}Po			
R-18	20190827	0.9	3.880	8.060	0.577	0.142 ± 0.021	0.295 ± 0.018	0.0211 ± 0.0046	23.3	2.08	0.149

season^{-1} for ^{210}Po. From Figure 3B, we can see that the highest seasonal deposition flux was observed in summer 2018 for both ^{7}Be and ^{210}Pb, whereas the highest seasonal value for ^{210}Po was observed in winter 2018. The lowest seasonal deposition flux was observed in the fall of 2020 for both ^{7}Be and ^{210}Pb and in the winter of 2020 for ^{210}Po. We can still find that the seasonal variation during each year showed the highest value in summer, followed by spring, and the lowest value was seen during fall for ^{210}Pb and ^{7}Be. This was different from the reported data in Shanghai that showed the highest deposition fluxes in winter and spring for ^{210}Pb and ^{7}Be, respectively, and the lowest in summer for both nuclides (Du et al., 2015). The seasonal variation for ^{210}Po was not obvious, and the maximum and minimum values may occur simultaneously in the same season of different years. The seasonal deposition fluxes of ^{210}Pb and ^{7}Be also varied during the same season of different years, with a maximum coefficient of variation of 45.34% being reported in the summer for ^{210}Pb and 48.37% for ^{7}Be in the winter.

The total deposition fluxes of ^{7}Be, ^{210}Pb, and ^{210}Po on the coast of the Maowei Sea were, respectively, 484, 199, and 99.4 Bq m^{-2} yr^{-1} for 2019 and 520, 190, and 26.2 Bq m^{-2} yr^{-1} for 2021. No significant difference was observed for ^{7}Be and ^{210}Pb. Atmospheric input of ^{7}Be, ^{210}Pb, and ^{210}Po on the Maowei Sea water surface could be estimated to be 6.53×10^{10}, 2.69×10^{10}, and 1.34×10^{10} Bq yr^{-1} in 2019 and 7.02×10^{10}, 2.56×10^{10}, and 0.35×10^{10} Bq yr^{-1} in 2021 by multiplying the surface area of the Maowei Sea. If we consider the total sampling months into two parts as before the COVID-2019 pandemic and after the COVID-2019 pandemic, an obvious reduction was found after COVID-2019, which deserved a long-term observation.

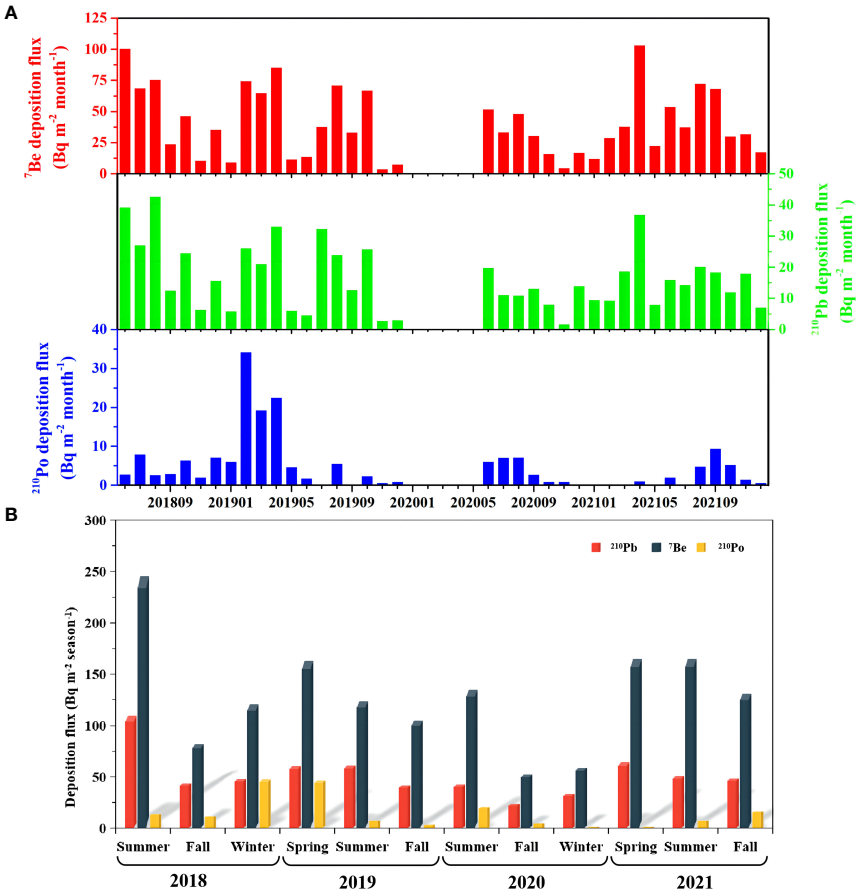

FIGURE 3
The temporal distribution pattern of monthly deposition fluxes for ^{7}Be, ^{210}Pb, and ^{210}Po (**A**, unit: Bq·m^{-2}·$month^{-1}$); and the distribution of seasonal deposition fluxes for ^{7}Be, ^{210}Pb, and ^{210}Po (**B**, unit: Bq·m^{-2}·$season^{-1}$).

4.3 Volume-weight activities of ^{7}Be, ^{210}Pb, and ^{210}Po

We defined the volume-weighted activity of a specific nuclide in the atmosphere as the amount of the nuclide divided by the rainfall data (Equation (8)). We found that the activity (Bq L^{-1}) of ^{7}Be varied from 0.05 ± 0.00 to 6.24 ± 0.37 with an average of 0.63 ± 1.07 (n=38) during our sampling period, which was much lower than the reported ^{7}Be activity in rainwater of different cities, such as Shanghai, China (1.34 Bq L^{-1}, Zhong, 2020), Xiamen, China (1.48-2.10 Bq L^{-1}, Chen et al., 2016; Zhang et al., 2016), and Hakodate, Japan (4.07 Bq L^{-1}, Tokieda et al., 1996). During the sampling period, the volume-weighted activity (Bq L^{-1}) of ^{210}Pb ranged from 0.01 ± 0.00 to 4.86 ± 0.73 with a mean of 0.35 ± 0.80 (n=38), which was close to the observation in Xiamen, China during 2010-2012 (0.375 Bq L^{-1}, Wang et al., 2014), but lower than the reported data in Japan [from 0.49 Bq L^{-1} in Hakodate during 1990-1991 (Tokieda et al., 1996) of 1.22 Bq L^{-1} in Assabu during 1972 (Tsunogai and Fukuda, 1974)]. The variation of the volume-weighted activity (Bq L^{-1}) for ^{210}Po ranged from 0.00 ± 0.00 to 0.55 ± 0.05 with an average of 0.07 ± 0.13 (n=38), which was much higher than the reported ^{210}Po activity concentrations in rainwater of different areas, such as Harwell, UK (0.009 Bq L^{-1}, Burton and Stewart, 1960), Arkansas and Boulder, USA (0.0058 and 0.0185 Bq L^{-1}, Poet et al., 1972; Gavini et al., 1974), Hakodate and Assabu, Japan (0.035 and 0.0098 Bq L^{-1}, Tsunogai and Fukuda, 1974), and Shanghai and Xiamen, China (0.0048 and 0.034 Bq L^{-1}, Wang et al., 2014; Chen et al., 2016; Zhong, 2020). No significant difference (p>0.05) was observed among different sampling years for ^{7}Be and ^{210}Pb. However, a significant difference (p<0.05) was found for ^{210}Po activity between different sampling years (June 2018-July 2019 and June 2020-July 2021). A much lower average ^{210}Po activity was obtained during June 2020-July 2021 than in June 2018-July 2019. A significant linear relationship was found between the activities of ^{210}Pb and ^{7}Be (r=0.980, p<0.0001, n=38), but no significant relationships were found between the activities of ^{210}Po and ^{210}Pb, or between ^{210}Po and ^{7}Be, indicating precipitation may be the main factor that influences the environmental behavior of ^{210}Pb and ^{7}Be, but not ^{210}Po. Generally, the order of activities for these three radionuclides was ^{210}Po<^{210}Pb<^{7}Be.

The temporal variations for activities of ^{7}Be, ^{210}Pb, and ^{210}Po during the study period are shown in Figure 4A. As seen in Figure 4A, the maximum activity values of ^{210}Pb and ^{7}Be were observed in January 2021 and the minimum value for ^{210}Pb was registered in August 2020, and for ^{7}Be it was seen in May 2019. However, there was also a much lower activity in August 2020 for ^{7}Be. The highest activity for ^{210}Po was observed in April 2019. Almost 85% of the deposition samples showed an activity of ^{210}Po of less than 0.1 Bq L^{-1}. Much similar temporal distribution patterns for the activities of all three radionuclides were found during our sampling period, that is, the activities started increasing in the fall of 2018, and reached the first peak in the spring of 2019, then suddenly decreased in the summer before another peak appeared in the fall of 2019. The variations repeated the same patterns in the following two years. In general, the variation of the activities for ^{7}Be and ^{210}Pb within the years 2019 and 2021 was shaped like a positive parabola, showing high values at the end of the year and low values during the middle of the year. The monthly volume-weighted activities of ^{7}Be and ^{210}Pb varied the most in January, with the maximum coefficient of variation of 125% and 128% for ^{7}Be and ^{210}Pb, respectively. The minimum coefficient of variation was found in March for both ^{7}Be and ^{210}Pb, with values of 8% and 21%, respectively. The maximum and minimum coefficients of variation for ^{210}Po were found in July and June with values of 142% and 39%, respectively.

The seasonal volume-weighted activity was obtained by dividing the total rainfall of a specific season into the total amount of nuclides during that specific season. The seasonal volume-weighted activities of ^{7}Be, ^{210}Pb, and ^{210}Po are shown in Figure 4B and indicate that the maximum seasonal volume-weighted activities were observed in the winter of 2018 for all three nuclides, and the minimum seasonal volume-weighted activities were observed in the fall of 2020 for ^{7}Be, in the summer of 2020 for ^{210}Pb, and in the spring of 2021 for ^{210}Po. The seasonal variations during each year showed high values in winter, followed by spring, and low values in summer, which indicated the dilution of the precipitation in summer (Du et al., 2015). Maximum coefficients of variation of 45% were found in summer for ^{210}Pb, and 48% and 139% in winter for both ^{7}Be and ^{210}Po, respectively. Minimum coefficients of variation of 0.8% and 3.7% were observed in spring for both ^{7}Be and ^{210}Po, respectively, and 50% in summer for ^{210}Po.

4.4 ^{7}Be/^{210}Pb and ^{210}Po/^{210}Pb activity ratios

The activity ratios of ^{7}Be/^{210}Pb and ^{210}Po/^{210}Pb can provide information about the vertical movements of air masses, the residence time of the airborne particulate matter in the atmosphere, and the scavenging of aerosols (Leppänen, 2019). In the 38 monthly deposition samples, the activity ratio of ^{7}Be/^{210}Pb varied from 1.17 to 4.35 with an average of 2.45 (n=38); the activity ratio of ^{210}Po/^{210}Pb varied from 0.00 to 1.31 with a mean value of 0.31 (n=38). The activity ratio of ^{210}Po/^{210}Pb was lower than that of ^{7}Be/^{210}Pb, and less than 1 for almost all the samples except for two samples, showing a defect for ^{210}Po compared to its parent ^{210}Pb. The activity ratio of ^{7}Be/^{210}Pb was greater than 1 in all samples. More than 50% of the deposition samples showed an activity ratio value of ^{7}Be/^{210}Pb between 2 and 3, and more than 30% of the samples had a value between 1 and 2. There was no significant difference (p>0.05) for both activity ratios of ^{210}Po/^{210}Pb and ^{7}Be/^{210}Pb among different sampling years. The activity ratio of ^{7}Be/^{210}Pb on the coast of the Maowei Sea was much different from the reported data in other regions, ranging from 1.3 to 30 in Malaga, Spain (Dueñas et al., 2017), from 2.2 to 14 in the Arctic region (Baskaran and Shaw, 2001), from 1.2 to 10.1 on the coastal region of Niteroi, Brazil (Sanders et al., 2011), and from 1.1 to 13.3 in Shanghai, China (Du et al., 2015). The relatively stable ratios reported on the coast of the Maowei Sea may indicate that atmospheric processes did not change frequently.

Figure 4C is a plot of the monthly volume-weighted activity ratios for ^{7}Be/^{210}Pb and ^{210}Po/^{210}Pb, from which we can see that

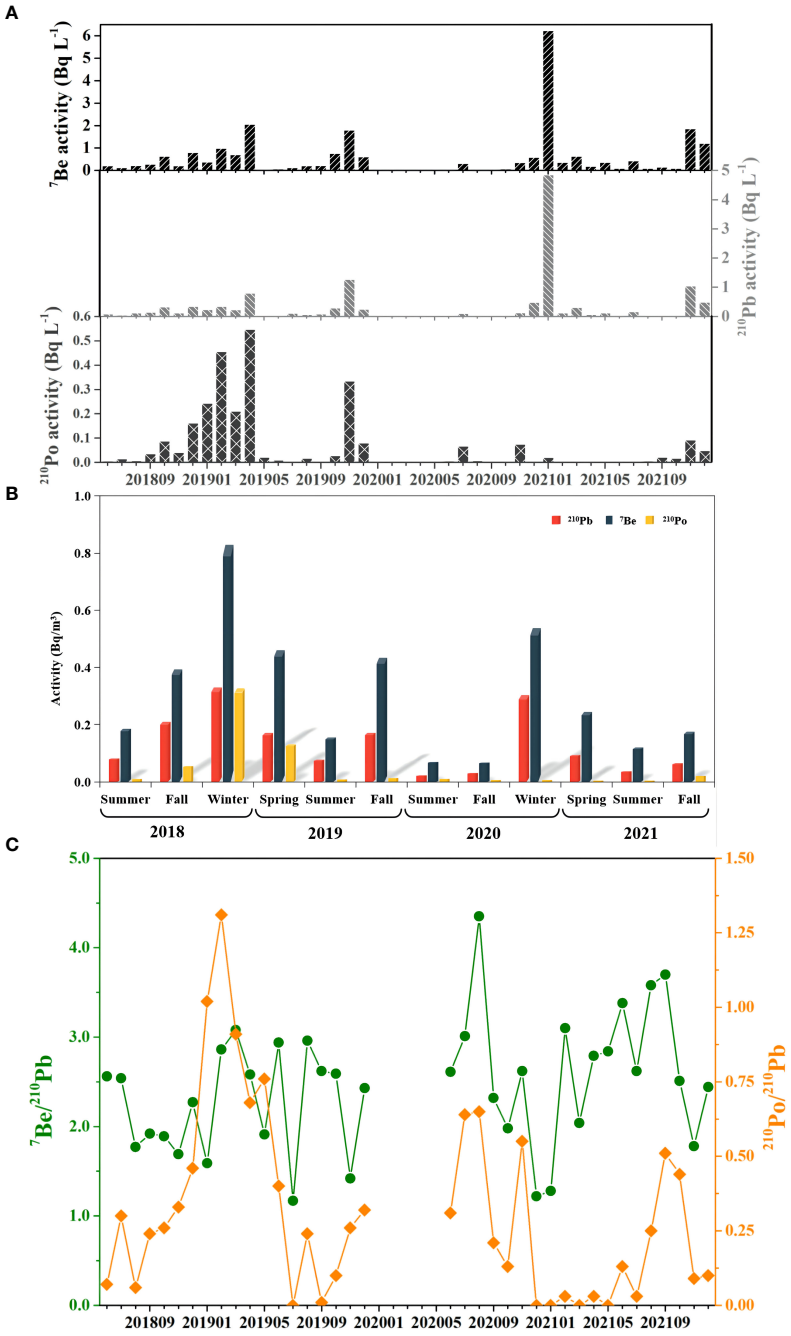

FIGURE 4
The temporal variations for monthly volume-weighted activities **(A)**, seasonal volume-weighted activities **(B)** of ^{7}Be, ^{210}Pb, and ^{210}Po, activity ratios of ^{7}Be/^{210}Pb and ^{210}Po/^{210}Pb **(C)** during the study period.

there was no consistent monthly variation trend for ratios of ^{7}Be/^{210}Pb and ^{210}Po/^{210}Pb. However, when a high activity ratio for ^{7}Be/^{210}Pb appeared, the activity ratio for ^{210}Po/^{210}Pb also showed a high value, which may indicate that the months with higher levels of ^{7}Be in the air were also the months with a longer residence time of atmospheric particulate matter. The highest value for ^{7}Be/^{210}Pb was found in August 2020 and the lowest in July 2019. ^{7}Be/^{210}Pb activity ratios did not show much variation in the same month of different years, with a maximum coefficient of variation of 34.4% in August, and a minimum of 5.6% in April. Seasonal ^{7}Be/^{210}Pb activity ratios ranged from 1.77 to 3.24 with an average of 2.46 (coefficient of variation of 18.8%), which was observed to be higher during summer 2021 and lower during winter 2020. The highest value for ^{210}Po/^{210}Pb was found in February 2019. Except for January and February 2019, the activity ratios of ^{210}Po/^{210}Pb were less than 1.0, indicating a defect of ^{210}Po compared to its parent ^{210}Pb. Unlike ^{7}Be/^{210}Pb activity ratios, ^{210}Po/^{210}Pb activity ratios showed many variations in the same month of different years, with a maximum coefficient of variation of 123% in July, and a minimum of 62% in November. Seasonal ^{210}Po/^{210}Pb activity ratios

ranged from 0.01 to 0.99 with an average of 0.30 (coefficient of variation of 100%), which was observed to be higher during the winter of 2018 and lower during the winter of 2020. The relatively stable ratios of $^{7}Be/^{210}Pb$ on the coast of the Maowei Sea may indicate atmospheric processes did not change frequently between different seasons.

4.5 Single rainfall

From the monthly precipitation shown in Figure 1, we can find that the distribution of rainfall throughout the year was uneven, with more than 80% of rainfall occurring in summer and only approximately 20% in winter. Therefore, it was necessary to study the specific rainfalls during the rainy season in order to study the influence of the precipitation on the nuclides' deposition. From June to August 2019, the rainiest months in 2019, 18 samples for single rainfall were collected. Table 2 and Figure 5 show the details of the total precipitation, deposition fluxes, and activities of ^{7}Be, ^{210}Pb, and ^{210}Po measured during these specific rainfalls on the coast of the Maowei Sea, Beibu Gulf, China. From this, we can see that the deposition fluxes and the activities varied with the precipitation. There was a positive relationship between the daily deposition fluxes and the precipitation, while a negative correlation was found between the activities and the precipitation. The activities (Bq L^{-1}) of ^{7}Be, ^{210}Pb, and ^{210}Po in specific rainfalls ranged from 0.03 ± 0.00 to 4.86 ± 0.29, 0.01 ± 0.00 to 1.94 ± 0.29, and 0.00 ± 0.00 to 0.29 ± 0.01 with the mean (n=18) of 0.63, 0.20, and 0.03, respectively. By comparison with the reported data in rainwater of different cities in the world, the activities of ^{7}Be and ^{210}Pb in rainwater on our study site were much lower than the average (2.25 Bq L^{-1} for ^{7}Be and 0.36 Bq L^{-1} for ^{210}Pb, Zhong, 2020); but the activity of ^{210}Po was much higher than the average reported data (0.018 Bq L^{-1}, Zhong, 2020). The activity ratio of $^{7}Be/^{210}Pb$ in these single rainfalls varied from 1.19 to 7.35 with an average of 3.22 (n=18). The activity ratio of $^{210}Po/^{210}Pb$ ranged from 0.07 to 0.90 with a mean of 0.18 (n=18) in these single rainfalls. The highest activity for all these three radionuclides was observed in sample R-17 collected on 26 August 2019, and the lowest for ^{7}Be and ^{210}Pb was observed in sample R-7 collected on 3 July 2019. For ^{210}Po, it was observed in sample R-6 collected on 1 July 2019. The precipitation during sampling was found to have the highest value on 1 July 2019, and a lower value on 26 August 2019, which may verify the dilution effect of rainfall. In 2019, the single rainfall events in June, July, and August brought about 24.5% of the total annual precipitation, but deposited approximately 24.8%, 17.7%, and 5.43% of the total annual bulk deposition fluxes of ^{7}Be, ^{210}Pb, and ^{210}Po, respectively, which may indicate that more ^{7}Be could be removed from the atmosphere by a single rainfall. Otherwise, the average precipitation for single rainfall was higher in June and lower in August, and the deposition flux was higher in June and lower in August as well, except for ^{210}Po, which was higher in August and lower in July. The activity showed higher values in August and low values in July, which indicated a further dilution of the precipitation for these radionuclides. The cumulative deposition, cumulative activity, and activity ratio can be calculated from the view of the time series for the single rainfall in one month and are shown in Figure 6. We can see that in all three months, a positive correlation was observed between the cumulative deposition of radionuclides and the elapsed time from the first single rainfall in each month (Figures 6A, D, G). However a logarithmic correlation was shown in June, and an exponential correlation in July and August. The relationship between cumulative activities for the three radionuclides and the elapsed

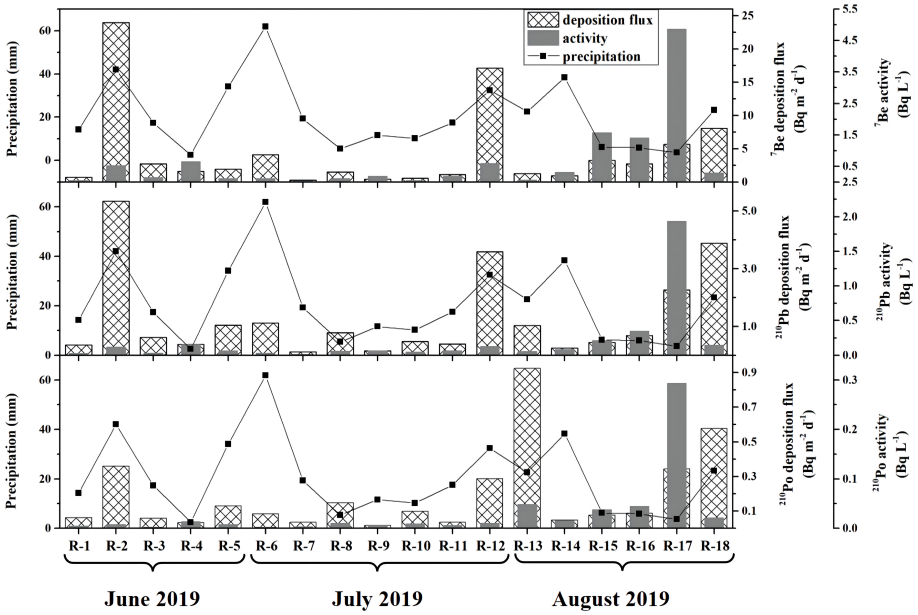

FIGURE 5
The details of the total precipitation, deposition fluxes, and activities of ^{7}Be, ^{210}Pb, and ^{210}Po measured during specific rainfalls in 2019 on the coast of the Maowei Sea, Beibu Gulf, China.

time showed a similar correlation as the cumulative relationship between deposition and elapsed time, except for ^{210}Po in August, which had a higher activity at first (Figure 6H). The activity ratio of ^{210}Po/^{210}Pb for the cumulative activities showed a general decline over time, while the activity ratio of ^{7}Be/^{210}Pb increased with the elapsed time in June and August. It was much different than the activity ratio of ^{210}Po/^{210}Pb for the cumulative activities, which first rose then fell over time, and the activity ratio of ^{7}Be/^{210}Pb, which went down and then up with time in July. Of all these single rainfall events, July registered the maximum rainfall intensity but the minimum cumulative deposition and activities for all three radionuclides despite their different origins and transport pathways in the atmosphere.

4.6 Sources and migration of the air masses for a single rainfall

In this study, the HYSPLIT model (Hybrid Single Particle Lagrangian Integrated Trajectory model) developed by the NOAA (National Oceanic and Atmospheric Administration) was used to analyze the sources of air masses during every single rainfall of our sampling period. The backward trajectory was calculated at heights 1.5 km, 5 km, and 12 km above mean sea level, starting from every specific sampling time, which was converted to the UTC (abbreviation for Universal Time Coordinated) time, ending at 72 h before the sampling time. The height of 1.5 km was assumed to represent the base of the precipitation cloud (Li, 2009) and the transportation of air masses was through the lower atmospheric layer. The altitude of 5 km was selected to analyze the migration of atmospheric air masses in the middle troposphere. The 12 km was set as the top layer of the model to analyze the movement of atmospheric masses between the tropopause and the lower stratosphere (Peng et al., 2011). Figure 7 shows the results of the backward trajectory analyses model, from which, we can see that the air masses were somewhat similar in the lower atmospheric layer (1.5 km, Figure 7A) and the middle troposphere (5 km, Figure 7B). Most of them were maritime air masses from the Beibu Gulf and the South China Sea, and some of them were mixed with continental air masses in the process of their transportation to the sampling site. However, the model results for the height of 12 km showed mainly continental air masses from the north and the west (Figure 7C). The ^{7}Be/^{210}Pb ratios of the single rainfall ranged from 1.19 (on 10 July 2019) and 7.35 (on 20 August 2019) with an average of 3.22, which was higher than the monthly and seasonal activity ratios. This may be due to the changes in the air masses during a single rainfall. In addition, the air mass backward trajectories on both 10 July and 4 August (with an activity ratio of 1.25) showed the vertical air masses moved from the tropopause to the lower stratosphere, which led to a lower ^{7}Be/^{210}Pb ratio in the sampling site. However, the backward trajectory on 20 August 2019 showed the sampling site was mainly influenced by the air mass in the lower atmosphere and mainly by the maritime air mass of Beibu Gulf in the south. Since the maritime air mass generally derived with a high ^{7}Be/^{210}Pb ratio (Du et al., 2015; Du, 2019; Peng et al., 2019), the source of this sample was mainly from the maritime air mass of Beibu Gulf in the lower atmospheric layer.

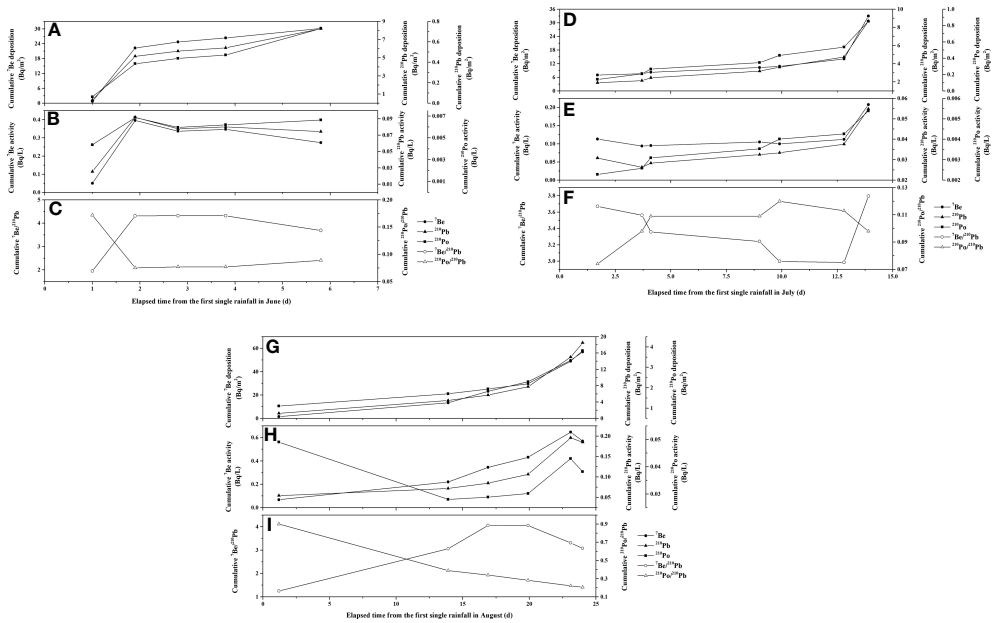

FIGURE 6
Cumulative depositions, cumulative activities, and activity ratios as time elapsed from the first single rainfall in June **(A–C)**, July **(D–F)**, and August **(G–I)** during 2019.

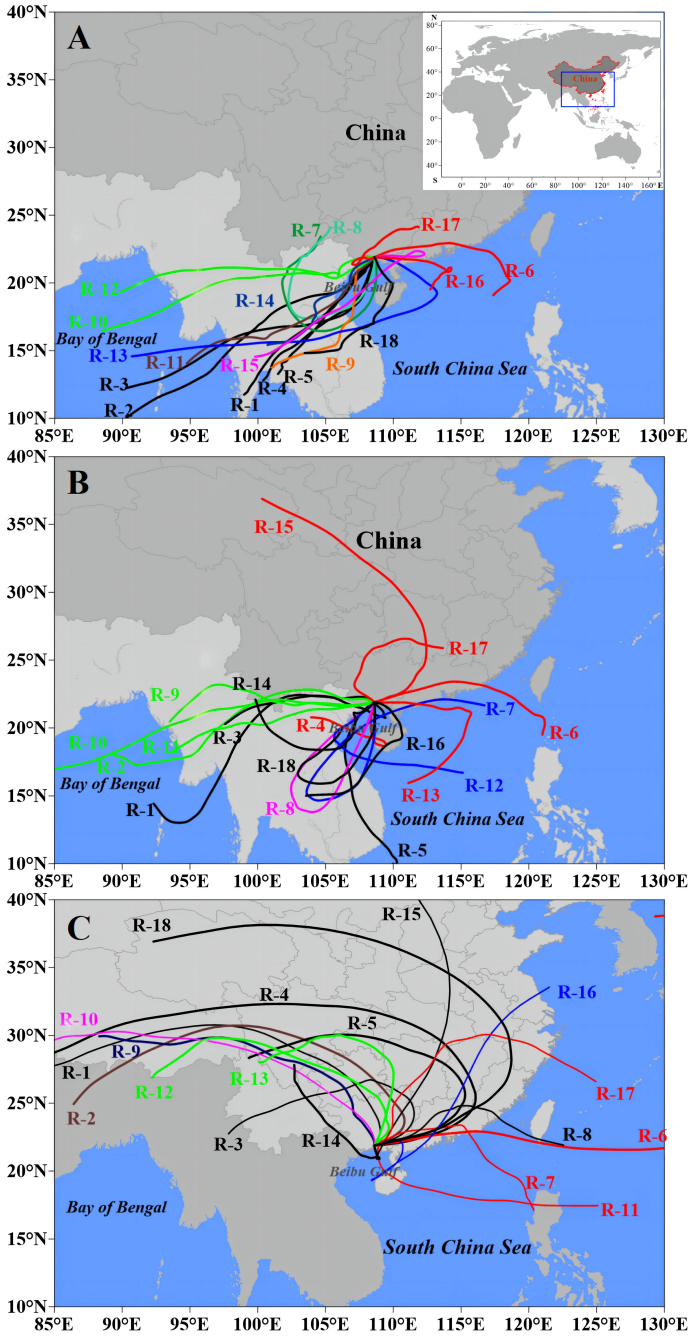

FIGURE 7
Air masses backward trajectory analyses of the specific rainfall events from R-1 to R-18 in different heights **(A)** 1.5 km, **(B)** 5.0 km, and **(C)** 12 km. Using different line colors to distinguish different rainfall events.

4.7 Factors influencing atmospheric deposition of radionuclides

When we attempted to investigate the factors influencing the atmospheric depositions of ^{7}Be, ^{210}Pb, and ^{210}Po, the levels of precipitation, AQI, the concentrations of particulate matters (PM, including $PM_{2.5}$ and PM_{10}), SO_2, NO_2, CO, and O_3 were assumed to explain the ambient air nuclides behavior in the present study. Figure 8 was a Pearson correlation matrix result of those possible environmental factors and the studied variables during our sampling period at the Maowei Sea coast. The color bar represents the correlation coefficients converted to percentages as shown in the correlation plot. Variables with significant correlations at a 95% confidence level ($p< 0.05$) are denoted by an asterisk (*)-marked. From Figure 8, we can see that the deposition flux and activity of ^{7}Be showed a strong positive correlation with the deposition flux and activity of ^{210}Pb, respectively, indicating a similar scavenging behavior for ^{7}Be and ^{210}Pb from the atmosphere. At the same time, the deposition flux and activity of ^{210}Po also showed positive correlations with the deposition fluxes

and activities of ^{210}Pb and ^{7}Be, respectively. However, the correlation between ^{210}Po and ^{210}Pb was not significant when compared with the correlation between ^{210}Po and ^{7}Be. Since the ^{210}Po/^{210}Pb activity ratio can trace the residence time of PM in the air, this further confirmed that a longer residence time of PM made it able to adsorb the particle reactive radionuclides in the air and generated higher deposition results. From Figure 8, precipitation, AQI, and PM (both $PM_{2.5}$ and PM_{10}) were the major factors that may influence the deposition of the three radionuclides. Precipitation had significant positive correlations with the deposition fluxes of all three radionuclides, indicating that rainfall was the main scavenging way from the atmosphere for these radionuclides. Meanwhile, both AQI and PM had significant negative correlations with the deposition fluxes of all three radionuclides, indicating that particle settlement could also remove the radionuclides in the air. The particle settlement was strongly affected by the precipitation (a significant negative correlation between AQI, PM, and the precipitation in Figure 8). This suggests that the total nuclide deposition might be the result of the scavenging of PM by precipitation. To further confirm the aforementioned hypothesis, the products of $PM_{2.5}$ and precipitation, PM_{10} and precipitation were used. The ^{7}Be and ^{210}Pb deposition fluxes were found significantly dependent on the arithmetic product of the PM level and precipitation. This demonstrated that PM was representative of the atmospheric ^{7}Be and ^{210}Pb levels and the scavenging of radionuclides was from atmospheric PM by precipitation. For ^{210}Po, although there was a positive correlation relationship between the deposition and the PM×precipitation, it was not significant, which indicates that it may depend on its production rate from ^{210}Pb and the residence time of the PM. Otherwise, the concentrations of SO_2, NO_2, and O_3 showed slightly weak negative correlations with the nuclide deposition, indicating, except for the decay of ^{222}Rn, that other sources, such as the burning of fossil fuels, could contribute ^{210}Pb and ^{210}Po in the atmosphere. Meanwhile, the level of O_3 can prevent some short rays from reaching the ground, so it could impact the deposition of ^{7}Be.

By combining all reported data listed in Table 1 in China, Figure 9 was constructed, from which, we can see that the latitude effect was obvious but different for all three radionuclides. For ^{7}Be, there was a positive correlation relationship between the annual deposition flux and the latitude, which may be due to the production of ^{7}Be in the atmosphere increasing with latitude (Usoskin and Kvaltsov, 2008) and the interaction between stratosphere and troposphere diminishing with decreasing latitude (Du et al., 2008). Except for the latitude effect, precipitation and the concentrations of $PM_{2.5}$ and PM_{10} can also influence the deposition flux of ^{7}Be (Liu et al., 2001), while the impact of precipitation was not so strong as the $PM_{2.5}$ and PM_{10} (Figure 9), indicating that the particle matter in the atmosphere was an important isotopic carrier. Under the influence of monsoons, atmospheric particle matters from inland/sea/high latitudes may have been transported to other areas, where they settled to the surface, leading to a high deposition of the radionuclides. In contrast, there were negative correlations between the annual deposition flux and the latitude for both ^{210}Pb and ^{210}Po, which had never been reported before since it was expected that their deposition could not show the latitude effect like ^{7}Be (Yamamoto et al., 2006; Du et al., 2015). However, because of the small amount of data, the relationship should be studied further. Besides, there were strong positive correlations between precipitation and the deposition fluxes of ^{210}Pb and ^{210}Po (Figure 9), indicating rainfall was the major scavenging way for ^{210}Pb and ^{210}Po in the atmosphere. Since the concentrations for $PM_{2.5}$ and PM_{10} in the early years were not available, the relationship was not discussed in this study.

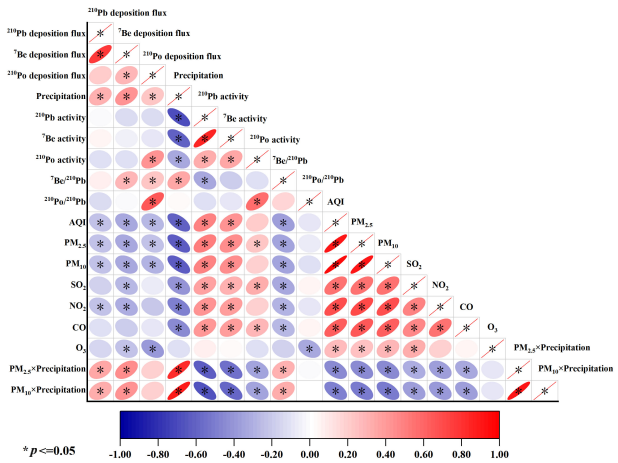

FIGURE 8
A Pearson correlation matrix result of the possible environmental factors and the studied variables during our sampling period at the Maowei Sea coast. The color bar represents the correlation coefficients converted to percentages as shown in the correlation plot. Variables with significant correlations at 95% confidence level ($p < 0.05$) are denoted by asterisk (*)-marked.

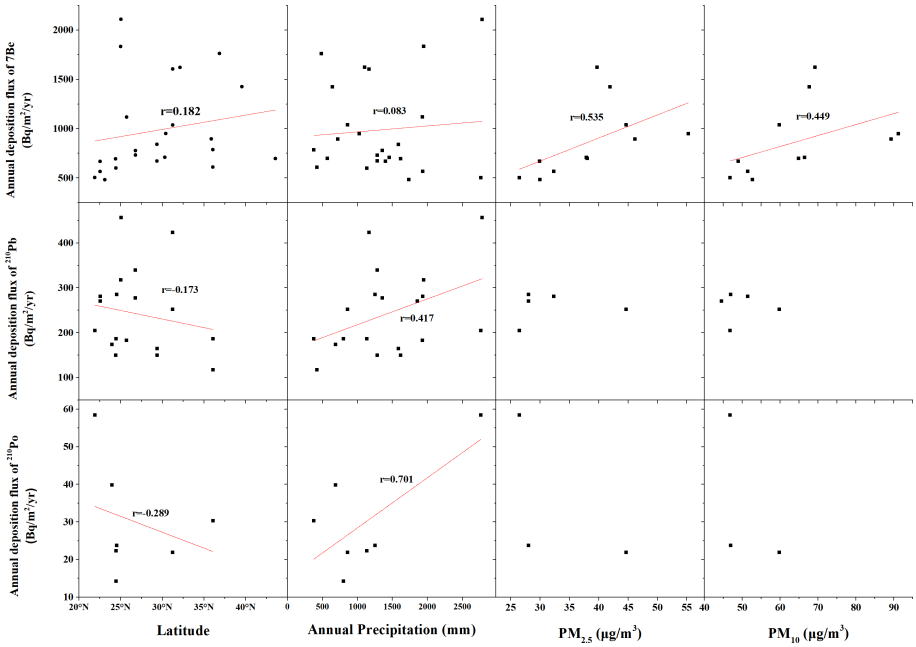

FIGURE 9
The correlations among the annual deposition fluxes for ^{7}Be, ^{210}Pb, and ^{210}Po with the latitude, precipitation, $PM_{2.5}$, and PM_{10} in China.

5 Conclusion

Based on the observations of ^{7}Be, ^{210}Pb, and ^{210}Po on the coast of the Maowei Sea from June 2018 to December 2021, the following conclusions can be made:

(1) The annual atmospheric depositional fluxes (Bq m^{-2} yr^{-1}) of ^{7}Be, ^{210}Pb, and ^{210}Po on the coast of the Maowei Sea were 496.80, 201.72, and 58.08, respectively. Both of the distributions for ^{7}Be and ^{210}Pb depositional fluxes during a whole year (the years 2019 and 2021) followed a bimodal pattern, with one peak from February to April and another peak from August to October, while the distribution for ^{210}Po depositional flux showed only one peak during the years of 2019 and 2021.

(2) The activities of ^{7}Be and ^{210}Pb were lower than the reported value in the rainwater of different cities, however, the activity of ^{210}Po was higher than the reported data in the rainwater of different cities.

(3) A Pearson correlation matrix and backward trajectory analysis for the specific single rainfall events showed that precipitation, AQI, PM (both $PM_{2.5}$ and PM_{10}), and the air masses movement during the rainfall were the major factors that may influence the deposition of ^{7}Be, ^{210}Pb, and ^{210}Po. A similar scavenging behavior was found for ^{7}Be, ^{210}Pb, and ^{210}Po from the atmosphere.

Data availability statement

The original contributions presented in the study are included in the article/supplementary material. Further inquiries can be directed to the corresponding author.

Author contributions

XW: Conceptualization, Methodology, Software, Data curation, Writing – original draft, Visualization, Investigation, Validation. JZ: Conceptualization, Methodology, Writing – review and editing, Validation, KS: Conceptualization, Methodology, Software, Data curation, Writing – review and editing, Visualization, Validation. JZD: Conceptualization, Methodology, Writing – review and editing, Validation, Supervision. LW: Conceptualization, Methodology, Investigation, Data curation, Writing – review and editing, Investigation, Validation. XL: Conceptualization, Methodology, Writing – review and editing, Investigation, Validation. DL: Conceptualization, Methodology, Writing –

review and editing, Validation, Supervision. All authors contributed to the article and approved the submitted version.

Funding

This work was supported by the National Natural Science Foundation of China (Nos. 41906150, 42107251), Open Found Project of Key Laboratory of Global Change and Marine-Atmospheric Chemistry (GCMAC2208), the Natural Science Foundation of Guangxi (Nos. 2021GXNSFDA075004, 2018GXNSFBA281051), Science and Technology Plan Projects of Guangxi Province (No. Gui Science AD19245147), and First-class Discipline Construction Project of Beibu Gulf University (No. DRA003).

Conflict of interest

The authors declare that the research was conducted in the absence of any commercial or financial relationships that could be construed as a potential conflict of interest.

Publisher's note

References

Baskaran, M. (2011). Po-210 and Pb-210 as atmospheric tracers and global atmospheric Pb-210 fallout: a review. *J. Environ. Radioactivity* 102 (5), 500–513. doi: 10.1016/j.jenvrad.2010.10.007

Baskaran, M., Coleman, C. H., and Santschi, P. H. (1993). Atmospheric depositional fluxes of ^{7}Be and ^{210}Pb at Galveston and college station, Texas. *J. Geophys. Res.: Atmospheres* 98 (D11), 20555–20571. doi: 10.1029/93JD02182

Baskaran, M., and Krupp, K. (2021). Novel application of ^{210}Po-^{210}Pb disequilibria to date snow, melt pond, ice core, and ice-rafted sediments in the Arctic ocean. *Front. Mar. Sci.* 8, 692631. doi: 10.3389/fmars.2021.692631

Baskaran, M., and Santschi, P. H. (2002). Particulate and dissolved ^{210}Pb activities in the shelf and slope regions of the gulf of Mexico waters. *Continental Shelf Res.* 22 (10), 1493–1510. doi: 10.1016/S0278-4343(02)00017-1

Baskaran, M., and Shaw, G. E. (2001). Residence time of arctic haze aerosols using the concentrations and activity ratios of ^{210}Po, ^{210}Pb and ^{7}Be. *J. Aerosol Sci.* 32 (4), 443–452. doi: 10.1016/S0021-8502(00)00093-8

Baskaran, M., and Swarzenski, P. W. (2007). Seasonal variations on the residence times and partitioning of short-lived radionuclides (^{234}Th, ^{7}Be and ^{210}Pb) and depositional fluxes of ^{7}Be and ^{210}Pb in Tampa bay, Florida. *Mar. Chem.* 104 (1–2) 27–42. doi: 10.1016/j.marchem.2006.06.012

Bi, Q. (2013). The disequilibrium of ^{234}Th/^{238}U and ^{210}Po/^{210}Pb in the changjiang estuary and adjacent sea: a case study of tracing the export of particulate organic carbon (in Chinese with English abstract) (Shanghai: East China Normal University).

Bronson, F. (2003). Validation of the accuracy of the LabSOCS software for mathematical efficiency calibration of Ge detectors for typical laboratory samples. *J. Radioanalytical Nucl. Chem.* 255 (1), 137–141. doi: 10.1023/A:1022248318741

Burton, W. M., and Stewart, N. G. (1960). Use of long-lived natural radioactivity as an atmospheric tracer. *Nature* 186 (4725), 584. doi: 10.1038/186584a0

Chang, T., Wu, Z., Huang, L., Geng, J., Zhu, Z., and Wu, W. (2015). Community structures of fish larvae and its relation with environmental factors in the mangrove of maoweihai bay (in Chinese with English abstract). *J. Appl. Oceanogr.* 34 (2), 219–226. doi: 10.3969 / J.ISSN.2095-4972.2015.02.010

Chen, J., Luo, S., and Huang, Y. (2016). Scavenging and fractionation of particle-reactive radioisotopes ^{7}Be, ^{210}Pb and ^{210}Po in the atmosphere. *Geochim. Cosmochimica Acta* 188, 208–223. doi: 10.1016/j.gca.2016.05.039

Dai, Z., Du, J., Chu, A., and Zhang, X. L. (2011). Sediment characteristics in the north branch of the Yangtze estuary based on radioisotope tracers. *Environ. Earth Sci.* 62 (8), 1629–1634. doi: 10.1007/s12665-010-0647-7

DeMaster, D. J., McKee, B. A., Nittrouer, C. A., Qian, J., and Cheng, G. (1985). Rates of sediment accumulation and particle reworking based on radiochemical measurements from continental shelf deposits in the East China Sea. *Continental Shelf Res.* 4 (1-2), 143–158. doi: 10.1016/0278-4343(85)90026-3

Ding, M., Su, L., Liu, G., Zhu, J., Feng, J., and Zhang, H. (2017). Atmospheric depositional fluxes of ^{7}Be and depositional velocities of aerosols in shenzhen (in Chinese with English abstract). *Geochimica* 46 (1), 81–86. doi: 10.19700/j.0379-1726.2017.01.007

Du, J. (2019). Study on the depositional processes of the atmospheric fallout radionuclides and their application on tracing modern sedimentation processes at the East China Sea (in Chinese with English abstract) (Shanghai: East China Normal University).

Du, J., Baskaran, M., and Du, J. (2020). Atmospheric deposition of ^{7}Be, ^{210}Pb and ^{210}Po during typhoons and thunderstorm in shanghai, China and global data synthesis. *Sci. China Earth Sci.* 063 (004), 602–614. doi: 10.1007/s11430-019-9481-9

Du, J., Du, J., Baskaran, M., Bi, Q., Huang, D., and Jiang, Y. (2015). Temporal variations of atmospheric deposition fluxes of ^{7}Be and ^{210}Pb over 8 years, 2006-2013) at shanghai, China and synthesis of global fallout data. *J. Geophys. Res.* 120 (9), 4323–4339. doi: 10.1002/2014JD022807

Du, J., Du, J. Z., Huang, D., Wang, J., and Zhang, J. (2016). Seasonal distribution patterns of ^{7}Be and ^{210}Pb in surface sediments in the changjiang estuary, China and their implication. *J. Mar. Syst.* 154, 41–49. doi: 10.1016/j.jmarsys.2015.05.001

Du, J., Wu, Y., Huang, D., and Zhang, J. (2010). Use of ^{7}Be, ^{210}Pb and ^{137}Cs tracers to the transport of surface sediments of the changjiang estuary, China. *J. Mar. Syst.* 82 (4), 286–294. doi: 10.1016/j.jmarsys.2010.06.003

Du, J., Zhang, J., and Wu, Y. (2008). Deposition patterns of atmospheric ^{7}Be and ^{210}Pb in coast of East China Sea, shanghai, China. *Atmospheric Environ.* 42 (20), 5101–5109. doi: 10.1016/j.atmosenv.2008.02.007

Dueñas, C., Gordo, E., Liger, E., Cabello, M., Cañete, S., Pérez, M., et al. (2017). ^{7}Be, ^{210}Pb and ^{40}K depositions over 11 years in málaga. *J. Environ. Radioactivity* 178, 325–334. doi: 10.1016/j.jenvrad.2017.09.010

Dutkiewicz, V. A., and Husain, L. (1985). Stratospheric and tropospheric components of ^{7}Be in surface air. *J. Geophys. Res.: Atmospheres* 90 (D3), 5783–5788. doi: 10.1029/JD090iD03p05783

Feng, H., Cochran, J. K., and Hirschberg, D. J. (1999a). ^{234}Th and ^{7}Be as tracers for the transport and dynamics of suspended particles in a partially mixed estuary. *Geochim. Cosmochimica Acta* 63 (17), 2487–2505. doi: 10.1016/S0016-7037(99)00060-5

Feng, H., Cochran, J. K., and Hirschberg, D. J. (1999b). ^{234}Th and ^{7}Be as tracers for the sources of particles to the turbidity maximum of the Hudson river estuary. *Estuarine Coast. Shelf Sci.* 49 (5), 629–645. doi: 10.1006/ecss.1999.0547

Fornes, W. L., DeMaster, D. J., Levin, L. A., and Blair, N. E. (1999). Bioturbation and particle transport in Carolina slope sediments: a radiochemical approach. *J. Mar. Res.* 57 (2), 335–355. doi: 10.1357/002224099321618245

Gai, N., Pan, J., Yin, X. C., Zhu, X. H., Yu, H. Q., Li, Y., et al. (2015). Latitudinal distributions of activities in atmospheric aerosols, deposition fluxes, and soil inventories of ^{7}Be in the East Asian monsoon zone. *J. Environ. Radioactivity* 148, 59–66. doi: 10.1016/j.jenvrad.2015.06.011

Gavini, M. B., Beck, J. N., and Kuroda, P. K. (1974). Mean residence times of the long-lived radon daughters in the atmosphere. *J. Geophys. Res.* 79 (30), 4447–4452. doi: 10.1029/JC079i030p04447

Huang, D. (2012). Applications of radionuclides to trace the sources, transport pathways and depositions of sediments in the changjiang estuary, East China Sea and coastal environment of eastern hainan island (in Chinese with English abstract) (Shanghai: East China Normal University).

Huang, D., Du, J., Moore, W. S., and Zhang, J. (2013). Particle dynamics of the changjiang estuary and adjacent coastal region determined by natural particle-reactive radionuclides (^{7}Be, ^{210}Pb, and ^{234}Th). *J. Geophys. Res.: Oceans* 118 (4), 1736–1748. doi: 10.1002/jgrc.20148

Huang, D., Du, J., Wu, Y., and Zhang, J. (2010). Sinking of particulates ^{234}Th$_{xs}$, ^{7}Be and ^{210}Pb$_{xs}$ in the changjiang estuary, China. *Chin. J. Oceanol. Limnol.* 28 (6), 1152–1159. doi: 10.1007/s00343-010-9036-z

Huang, J., Li, Y., Tao, W., Jing, K., and Chen, J. (2020). Equipment and data analysis of guangxi continuous wet weather observation system (in Chinese with English abstract). *J. Meteorological Res. Appl.* 41 (2), 89–92. doi: 10.19849/j.cnki.CN45-1356/P.2020.2.18

Jia, C., Liu, G., Yang, W., Zhang, L., and Huang, Y. (2003). Atmospheric depositional fluxes of ^{7}Be and ^{210}Pb at xiamen (in Chinese with English abstract). *J. Xiamen Univ. (Natural Science)* 42 (3), 352–357.

Kim, S. H., Hong, G. H., Baskaran, M., Park, M., Chung, C. S., and Kin, K. H. (1998). Wet removal of atmospheric ^{7}Be and ^{210}Pb at the Korean yellow Sea coast. *Yellow Sea* 4, 58–68.

Lal, D., Malhotra, P. K., and Peters, B. (1958). On the production of radioisotopes in the atmosphere by cosmic radiation and their application to meteorology. *J. Atmospheric Terrestrial Phys.* 12, 306–328. doi: 10.1016/0021-9169(58)90062-X

Lal, D., and Peters, B. (1967). "Cosmic ray produced radioactivity on the earth," in *Kosmische strahlung II/Cosmic rays II* (Berlin, Heidelberg: Springer), 551–612.

Lee, H. I., Huh, C. A., Lee, T., and Huang, N. E. (2015). Time series study of a 17-year record of ^{7}Be and ^{210}Pb fluxes in northern Taiwan using ensemble empirical mode decomposition. *J. Environ. Radioactivity* 147, 14–21. doi: 10.1016/j.jenvrad.2015.04.017

Leppänen, A. P. (2019). Deposition of naturally occurring ^{7}Be and ^{210}Pb in northern Finland. *J. Environ. Radioactivity* 208-209, 105995. doi: 10.1016/j.jenvrad.2019.105995

Li, Y. (2009). Acid deposition responsing of meteorological elements and air mass trajectories in liaozhong station (in Chinese with English abstract) (Shangdong: Shandong Normal University).

Liu, H., Jacob, D. J., Bey, I., and Yantosca, R. M. (2001). Constraints from 210Pb and 7Be on wet deposition and transport in a global three-dimensional chemical tracer model driven by assimilated meteorological fields. *J. Geophys. Res.: Atmospheres* 106 (D11), 12109–12128. doi: 10.1029/2000JD900839

Luo, X., Gu, M., Zhong, L., and Lin, Z. (2015). Causal analysis of typical "High-humidity weather" events in guangxi in recent years (in Chinese with English abstract). *Meteorological Sci. Technol.* 43 (4), 659–665. doi: 10.19517/j.1671-6345.2015.04.017

Marley, N. A., Gaffney, J. S., and Drayton, P. J. (2000). Measurement of ^{210}Pb, ^{210}Po and ^{210}Bi in size-fractionated atmospheric aerosols: an estimate of fine-aerosol residence times. *Aerosol Sci. Technol.* 32 (6), 569–583. doi: 10.1080/027868200303489

McKee, B. A., Nittrouer, C. A., and DeMaster, D. J. (1983). Concepts of sediment deposition and accumulation applied to the continental shelf near the mouth of the Yangtze river. *Geology* 11 (11), 631–633. doi: 10.1130/0091-7613(1983)11<631:COSDAA>2.0.CO;2

McNeary, D., and Baskaran, M. (2003). Depositional characteristics of ^{7}Be and ^{210}Pb in southeastern Michigan. *J. Geophys. Res.* 108 (D7), 4210–4224. doi: 10.1029/2002JD003021

McNeary, D., and Baskaran, M. (2007). Residence times and temporal variations of ^{210}Po in aerosols and precipitation from southeastern Michigan, united states. *J. Geophys. Res.: Atmospheres* 112, D04208. doi: 10.1029/2006JD007639

Moore, H. E., Poet, S. E., and Martell, E. A. (1973). ^{222}Rn, ^{210}Pb, ^{210}Bi, and ^{210}Po profiles and aerosol residence times versus altitude. *J. Geophys. Res.* 78 (30), 7065–7075. doi: 10.1029/JC078i030p07065

Nozaki, Y., Zhang, J., and Takeda, A. (1997). ^{210}Pb and ^{210}Po in the equatorial pacific and the Bering Sea: the effects of biological productivity and boundary scavenging. *Deep Sea Res. Part II: Topical Stud. Oceanogr.* 44 (9-10), 2203–2220. doi: 10.1016/S0967-0645(97)00024-6

Peirson, D. H., Cambray, R. S., and Spicer, G. S. (1966). Lead-210 and polonium-210 in the atmosphere. *Tellus* 18 (2-3), 427–433. doi: 10.3402/tellusa.v18i2-3.9381

Peng, L., Gao, W., Geng, F., Ran, L., and Zhou, H. (2011). Analysis of ozone vertical distribution in shanghai area (in Chinese with English abstract). *Acta Sci. Nat. Univ Peking* 47, 805–811.

Peng, A., Liu, G., Jiang, Z., Liu, G., and Liu, M. (2019). Wet depositional fluxes of ^{7}Be and ^{210}Pb and their influencing factors at two characteristic cities of China. *Appl. Radiat. Isotopes* 147, 21–30. doi: 10.1016/j.apradiso.2019.01.016

Poet, S. E., Moore, H. E., and Martell, E. A. (1972). Lead 210, bismuth-210, and polonium-210 in the atmosphere: accurate ratio measurement and application to aerosol residence time determination. *J. Geophys. Res.* 77 (33), 6515–6527. doi: 10.1029/JC077i033p06515

Qian, J., Wang, X., and Xu, Z. (1986). The Pb-210 atmospheric precipitation flux near the East China Sea (in Chinese with English abstract). *Donghai Mar. Sci.* 4 (1), 27–33.

Robbins, J. A. (1978). "Geochemical and geophysical applications of radioactive lead," in *The biogeochemistry of lead in the environment*. Ed. J. O. Nriagu (Elsevier/North-Holland Biomedical Press), 285–393.

Sanders, C. J., Smoak, J. M., Cable, P. H., Patchineelam, S. R., and Sanders, L. M. (2011). Lead-210 and beryllium-7 fallout rates on the southeastern coast of Brazil. *J. Environ. Radioactivity* 102 (12), 1122–1125. doi: 10.1016/j.jenvrad.2011.07.008

Shan, J. (2010). Research and application on methods for the residence time of atmospheric aerosol (in Chinese with English abstract) (Hunan: University of South China).

Shi, Z., Wen, A., Yan, D., Zhang, X., and Ju, L. (2011). Temporal variation of ^{7}Be fallout and its inventory in purple soil in the three gorges reservoir region, China. *J. Radioanalytical Nucl. Chem.* 288 (3), 671–676. doi: 10.1007/s10967-010-0934-5

Su, L. (2018). Trace study on the resident time and deposition velocity of airborne particulates using multi-nuclides in shenzhen (in Chinese with English abstract) (Shenzhen: Shenzhen University).

Su, K., Du, J., Baskaran, M., and Zhang, J. (2017). Po-210 and Pb-210 disequilibrium at the PN section in the East China Sea. *J. Environ. Radioactivity* 174, 54–65. doi: 10.1016/j.jenvrad.2016.07.031

Su, C. C., Huh, C. A., and Lin, F. J. (2003). Factors controlling atmospheric fluxes of ^{7}Be and ^{210}Pb in northern Taiwan. *Geophys. Res. Lett.* 30 (19), 2018. doi: 10.1029/2003GL018221

Tokieda, T., Yamanaka, K., Harada, K., and Tsunogai, S. (1996). Seasonal variations of residence time and upper atmospheric contribution of aerosols studied with Pb-210, bi-210, po-210 and be-7. *Tellus B* 48 (5), 690–702. doi: 10.3402/tellusb.v48i5.15940

Tsunogai, S., and Fukuda, K. (1974). Pb-210, bi-210 and po-210 in meteoric precipitation and the residence time of tropospheric aerosol. *Geochem. J.* 8, 141–152. doi: 10.2343/geochemj.8.141

Turekian, K. K., Benninger, L. K., and Dion, E. P. (1983). ^{7}Be and ^{210}Pb total deposition fluxes at new haven conneticut and at Bermuda. *J. Geophys. Res.* 88, 5411–5415. doi: 10.1029/JC088iC09p05411

Turekian, K. K., Nozaki, Y., and Benninger, L. K. (1977). Geochemistry of atmospheric radon and radon products. *Annu. Rev. Earth Planetary Sci.* 5 (1), 227–255. doi: 10.1146/annurev.ea.05.050177.001303

Usoskin, I. G., and Kovaltsov, G. A. (2008). Production of cosmogenic ^{7}Be isotope in the atmosphere: full 3-d modeling. *J. Geophys. Res.: Atmospheres* 113, D12107 doi: 10.1029/2007JD009725.

Wallbrink, P. J., and Murray, A. S. (1994). Fallout of ^{7}Be in south eastern Australia. *J. Environ. Radioactivity* 25 (3), 213–228. doi: 10.1016/0265-931X(94)90074-4

Wang, Z., Yang, W., Chen, M., Lin, P., and Qiu, Y. (2014). Intra-annual deposition of atmospheric ^{210}Pb, ^{210}Po and the residence times of aerosol in xiamen, China. *Aerosol Air Qual. Res.* 14 (5), 1402–1410. doi: 10.4209/aaqr.2013.05.0170

Wu, Y., Du, J., Huang, D., and Zhang, J. (2009). Gamma spectrum analysis of IAEA international intercomparison samples (in Chinese with English abstract). *J. Nucl. Radiochem.* 31 (3), 157–162.

Wu, J., Li, Y., Liu, G., Su, L., and Ding, M. (2021). Activity concentrations, depositional fluxes and deposition velocities of ^{210}Pb in atmospheric aerosols of shenzhen (in Chinese with English abstract). *Geochimica* 50 (2), 219–225. doi: 10.19700/j.0379-1726.2021.02.008

Wu, L., Ren, F., and Xu, S. (2020). Impact of first-level response to COVID-19 on the reduction of urban air pollutants in China (in Chinese with English abstract). *J. Environ. Economics* 3, 1–20. doi: 10.19511/j.cnki.jee.2020.03.001

Xia, S., Li, J., and Ni, Z. (2020). The impact of COVID-19 on china's social and economic development (in Chinese). *Cai Zhen Jian Du* 10, 5–9.

Yamamoto, M., Sakaguchi, A., Sasaki, K., Hirose, K., Igarashi, Y., and Kim, C. K. (2006). Seasonal and spatial variation of atmospheric ^{210}Pb and ^{7}Be deposition: features of the Japan Sea side of Japan. *J. Environ. Radioactivity* 86 (1), 110–131. doi: 10.1016/j.jenvrad.2005.08.001

Yang, B., Yang, H., Chen, J., Ding, Z., and Wang, X. (2012). Depositional fluxes of ^{7}Be at nanjing region (in Chinese with English abstract). *Resour. Environ. Yangtze Basin* 21 (11), 1376–1381.

Yang, F., Ye, B., He, K., Ma, Y., Cadle, S. H., Chan, T., et al. (2005). Characterization of atmospheric mineral components of $PM_{2.5}$ in Beijing and shanghai, China. *Sci. Total Environ.* 343, 221–230. doi: 10.1016/j.scitotenv.2004.10.017

Yi, Y., Bai, J., Liu, G., Yang, W., Yi, Q., Huang, Y., et al. (2005). Measurements of atmospheric deposition fluxes of ^{7}Be, ^{210}Pb and ^{210}Po (in Chinese with English abstract). *Mar. Sci.* 29 (12), 20–24.

Yi, Y., Zhou, P., and Liu, G. (2007). Atmospheric deposition fluxes of ^{7}Be, ^{210}Pb and ^{210}Po at xiamen, China. *J. Radioanalytical Nucl. Chem.* 273 (1), 157–162. doi: 10.1007/s10967-007-0728-6

Zhang, L. H., Yang, W. F., Chen, M., Wang, Z., Lin, P., Fang, Z. M., et al. (2016). Atmospheric deposition of ^{7}Be in the southeast of China: a case study in xiamen. *Aerosol Air Qual. Res.* 16 (1), 105–113. doi: 10.4209/aaqr.2015.03.0182

Zhang, L., Yang, W., Chen, M., Zhu, Y., and Wang, Z. (2019). Atmospheric deposition of ^{210}Po and ^{210}Pb near the coast of xiamen (in Chinese with English abstract). *Haiyang Xuebao* 41 (6), 114–122. doi: 10.3969/j.issn.0253-4193.2019.06.011

Zhang, F., Zhang, B., and Yang, M. (2013). Beryllium-7 atmospheric deposition and soil inventory on the northern loess plateau of China. *Atmospheric Environ.* 77, 178–184. doi: 10.1016/j.atmosenv.2013.05.002

Zheng, X., Shen, C., Wan, G., Liu, K., Tang, J., and Xu, X. (2010). ^{10}Be/^{7}Be implies the contribution of stratosphere-troposphere transport to the winter-spring surface O_3 variation observed on the Tibetan plateau (in Chinese with English abstract). *Chin. Sci. Bull.* 55 (35), 3403–3407. doi: 10.1007/s11434-010-4211-3

Zhong, Q. (2020). Atmospheric deposition of radionuclides and its application in POC export fluxes of the upper sea (in Chinese with English abstract) (Shanghai: East China Normal University).

Zhong, Q., Guo, W., Wang, H., Ji, J., Lin, J., Du, J., et al. (2023). ^{210}Po and ^{210}Pb as tracers for particle cycling in a shallow semi-enclosed bay of Taiwan strait. *Deep-Sea Res. Part II* 207, 105228. doi: 10.1016/j.dsr2.2022.105228

Zhong, Q., Puigcorbé, V., Sanders, C., and Du, J. (2020). Analysis of ^{210}Po, ^{210}Bi, and ^{210}Pb in atmospheric and oceanic samples by simultaneously auto-plating ^{210}Po and ^{210}Bi onto a nickel disc. *J. Environ. Radioactivity* 220, 106301. doi: 10.1016/j.jenvrad.2020.106301

Zhong, Q., Wang, J., Du, J., Bi, Q., and Zhao, F. (2019). The ^{210}Po/^{210}Pb disequilibrium in a spring-blooming marginal sea, the southern yellow Sea. *J. Environ. Radioactivity* 207, 15–26. doi: 10.1016/j.jenvrad.2019.05.017

Zhu, J., and Olsen, C. R. (2009). Beryllium-7 atmospheric deposition and sediment inventories in the neponset river estuary, Massachusetts, USA. *J. Environ. Radioactivity* 100 (2), 192–197. doi: 10.1016/j.jenvrad.2008.11.013

Zou, H., Su, X., Xu, X., Zeng, X., and Xu, P. (1982). Determination of recent sedimentation rates on the continental shelf of the East China Sea using ^{210}Pb method (in Chinese with English abstract). *Taiwan Strait* 1 (2), 30–40.